ResearchGate

See discussions, stats, and author profiles for this publication at: https://www.researchgate.net/publication/351296143

Cellulose Supported Magnetic Nanohybrids: Synthesis, Pysicomagnetic Properties and Biomedical Applications–A Review

Article *in* Carbohydrate Polymers · April 2021

DOI: 10.1016/j.carbpol.2021.118136

CITATION
1

READS
110

11 authors, including:

Mhd. Abd. Cader Mhd. Haniffa
University of Malaya
31 PUBLICATIONS **156** CITATIONS
SEE PROFILE

Khadija Munawar
University of Malaya
13 PUBLICATIONS **58** CITATIONS
SEE PROFILE

Ching Yern Chee
University of Malaya
117 PUBLICATIONS **2,446** CITATIONS
SEE PROFILE

Sumit Pramanik
University of Malaya
42 PUBLICATIONS **987** CITATIONS
SEE PROFILE

Some of the authors of this publication are also working on these related projects:

Bionanocomposite coating film with UV resistance and Self-cleaning properties for windows and vehicles. View project

"Modeling of the Atmospheric degradation of Volatile Organic Compounds in urban air sheds of Sri Lanka" View project

All content following this page was uploaded by Khadija Munawar on 21 May 2021.

The user has requested enhancement of the downloaded file.

Carbohydrate Polymers 267 (2021) 118136

Contents lists available at ScienceDirect

Carbohydrate Polymers

journal homepage: www.elsevier.com/locate/carbpol

Review

Cellulose supported magnetic nanohybrids: Synthesis, physicomagnetic properties and biomedical applications-A review

Mohamed Abdul Cader Mohamed Haniffa [a,*], Khadija Munawar [a,*], Ching Yern Chee [a,b,**], Sumit Pramanik [c], Ahmed Halilu [b], Hazlee Azil Illias [a,d,**], Muhammad Rizwan [e], Rajendram Senthilnithy [f], Kariyawasam Ranaweerage Ranjith Mahanama [g], Ashis Tripathy [h], Mohd Fahmi Azman [i]

[a] Centre of Advanced Manufacturing and Material Processing, Faculty of Engineering, University of Malaya, 50603 Kuala Lumpur, Malaysia
[b] Department of Chemical Engineering, Faculty of Engineering, University of Malaya, 50603 Kuala Lumpur, Malaysia
[c] Functional and Biomaterials Engineering Lab, Department of Mechanical Engineering, Faculty of Engineering and Technology, SRM Institute of Science and Technology, Kattankulathur, Kancheepuram, 603203, Chennai, Tamil Nadu, India
[d] Department of Electrical Engineering, Faculty of Engineering, University of Malaya, 50603 Kuala Lumpur, Malaysia
[e] Department of Chemistry, The University of Lahore, Lahore, Pakistan
[f] Department of Chemistry, Faculty of Natural Sciences, The Open University of Sri Lanka, 10250 Nawala, Nugegoda, Sri Lanka
[g] Department of Chemistry, Faculty of Science, University of Colombo, 0070 Colombo-3, Sri Lanka
[h] Center for MicroElectroMechanics Systems (CMEMS), University of Minho, Campus de Azurém, 4800-058 Guimarães, Portugal
[i] Physics Division, Centre for foundation studies, University of Malaya, 50603 Kuala Lumpur, Malaysia

ARTICLE INFO

Keywords:
Magneto-responsive cellulose
Cancer therapy
Drug delivery
MRI
Enzyme immobilization
Folate-conjugate

ABSTRACT

Cellulose and its forms are widely used in biomedical applications due to their biocompatibility, biodegradability and lack of cytotoxicity. It provides ample opportunities for the functionalization of supported magnetic nanohybrids (CSMNs). Because of the abundance of surface hydroxyl groups, they are surface tunable in either homogeneous or heterogeneous solvents and thus act as a substrate or template for the CSMNs' development. The present review emphasizes on the synthesis of various CSMNs, their physicomagnetic properties, and potential applications such as stimuli-responsive drug delivery systems, MRI, enzyme encapsulation, nucleic acid extraction, wound healing and tissue engineering. The impact of CSMNs on cytotoxicity, magnetic hyperthermia, and folate-conjugates is highlighted in particular, based on their structures, cell viability, and stability. Finally, the review also discussed the challenges and prospects of CSMNs' development. This review is expected to provide CSMNs' development roadmap in the context of 21st-century demands for biomedical therapeutics.

1. Introduction

Recent technological advancements and novel nano-architecture strategies have intrigued the interest of many researchers in improving the efficacy of conventional therapeutics in biomedical applications. In this context, magnetic nanoparticles (MNPs) are rapidly emerging as one of the most essential classes of functional nanomaterials in the biomedical field (Halilu et al., 2016; Halilu et al., 2019; Reddy et al., 2012; Umar et al., 2020). Due to nanoscale, low sedimentation rates, high active surface areas, optimized cellular diffusion, and controllable properties under an external magnetic field (EMF), MNPs are used in the field of hyperthermia, drug release, medical imaging, tissue engineering, and theranostic applications (Biliuta & Coseri, 2016). In general, MNPs have a decisive role in the encapsulation of both in vitro stability and in vivo performance (Biliuta et al., 2017). Therefore, the popular MNPs include ferromagnetic cobalt or iron, superparamagnetic Fe_3O_4 and Co_3O_4 (Pardo et al., 2020), ferrites (e.g., $BaFe_{12}O_{19}$, and $SrFe_{12}O_{19}$) (Davarpanah et al., 2019; Garg et al., 2020;

* Corresponding authors.
** Corresponding authors at: Centre of Advanced Manufacturing and Material Processing, Faculty of Engineering, University of Malaya, 50603 Kuala Lumpur, Malaysia.
E-mail addresses: mmmhaniffa@um.edu.my (M.A.C.M. Haniffa), khadija_munawar@um.edu.my (K. Munawar), chingyc@um.edu.my (C.Y. Chee), sumitprs@srmist.edu.in (S. Pramanik), h.illias@um.edu.my (H.A. Illias).

https://doi.org/10.1016/j.carbpol.2021.118136
Received 30 November 2020; Received in revised form 24 April 2021; Accepted 27 April 2021
Available online 30 April 2021
0144-8617/© 2021 Elsevier Ltd. All rights reserved.

Pham et al., 2020), and metal alloys (e.g., CoPt and FePt) (Pathak & Kashyap, 2021). Among these options, Fe_3O_4 NPs have extensively been used in biomedical applications compere to Fe_2O_3-based MNPs composites (Cardoso et al., 2018; Leonel et al., 2019; Li, Wei, et al., 2016). This differentiation in the usage of the Fe_3O_4 NPs is due to their superparamagnetic behavior, physicochemical stability, relatively low toxicity and biocompatibility at room temperature (RT). However, the magnetic dipole–dipole attractions between nanoparticles (NPs) cause them to agglomerate together and form large clusters, resulting in increased particle size. The MNPs with superparamagnetism are preferred for use in biomedical applications due to their rapid response to EMF; thus, to control the MNPs size smaller than 20 nm, they are hybridized into functional biomaterials like cellulose (Ge et al., 2009).

Cellulose is the most abundant carbohydrate on Earth, which is found 90% in cotton fiber, 40–50% in wood as well as approximately 57% in dried hemp. Cellulose is a fascinating biopolymer that at micro and nanoscale can serve as a functionalization surface. In contrast to other supporting functional biomaterials such as chitosan, alginate, graphene, hydroxyapatite (HA), and poly lactic-*co*-glycolic acid, cellulose has shown great potential to be used to hybridize MNPs in a variety of magnetic nanohybrids. It is because of its high specific surface area, low average aspect ratio (length to diameter) in the range of 15–80, abundant surface hydroxyl groups, and ample opportunities for surface functionalization in both homogeneous and heterogeneous solvent systems (Haniffa et al., 2020; Panchal et al., 2018; Williams et al., 2019).

Accordingly, various forms of cellulose, such as bacterial cellulose (BC), microcrystalline cellulose (MCC), cellulose nanofibril (CNF), and cellulose nanocrystals (CNC), as well as their promising surface modifications, have been widely used in the synthesis of various novel cellulose supported magnetic nanohybrids (CSMNs) (Li, Kaushik, et al., 2016; Liang et al., 2019; Lu et al., 2017; Matos et al., 2018; Sabaqian et al., 2017; Su et al., 2019). Carboxymethyl cellulose (CMC) is a modified form of cellulose used in many CSMNs' synthesis. It has also been recommended by the US Food and Drug Administration (FDA) for use in many applications, including controlled drug delivery systems, gene delivery nanocarriers, and food emulsifiers, and so on (Leonel et al., 2019; Mansur et al., 2018).

Since the initial fabrication of magnetic cellulosic fibers and paper based on the respective 'lumen loading' (Middleton & Scallan, 1985) and in situ synthesis techniques (Raymond et al., 1994), various CSMNs have already been reported in the literature. One-pot synthesis of CSMN using amine-rich magnetite and BC revealed that the presence of BC nanofibers had smoothened the growth and deposition of MNPs along the BC backbone (Nata et al., 2011). Sivakumar and co-workers reported a two-step synthesis of Fe_3O_4 nanoconjugate through dispersed Fe_3O_4 NPs in the drug-loaded and folate conjugated CMC suspension (Sivakumar et al., 2013). The results showed that the MNPs could act as "nano heaters" under an EMF and have potential applications in oncology therapy and drug delivery systems. Moreover, CMC has also been used in magnetic capture and hybridization processes to produce CSMN. These methods of mRNA isolation are faster, easier, and less expensive, with a high yield (Sarkar & Irudayaraj, 2008; Xiong et al., 2020). It is because of the stable electrostatic repulsions effectively formed between the MNPs and the carboxylic functional groups of CMC.

Essentially, there are various types of CSMNs including, nanorods (Abbasi Pour et al., 2017; Chen et al., 2014; Furlan et al., 2019), films (Dhar et al., 2016; Yoshitake et al., 2016), fibers (Pan et al., 2016; Williams et al., 2019), nanocarriers (Hosseini et al., 2020; Kanagarajan & Thiyagarajan, 2018), folate-conjugate (Sivakumar et al., 2013), hydrogel beads (Du et al., 2018; Karzar Jeddi & Mahkam, 2019), scaffolds (Torgbo & Sukyai, 2019), spheres (Peng et al., 2014), hydrogels (Naderi et al., 2020; Zhang, Jin, et al., 2018), microspheres (Gao et al., 2009), colloids (Leonel et al., 2019), and Pickering emulsion (Low et al., 2019; Low et al., 2018) with excellent magnetic, hyperthermic, drug release, folate-conjugation, cytotoxycity, electrical, exogenous (EMF) and endogenous (pH) stimuli-responsive properties, which lead them to be used in various potential biomedical applications.

In general, many detailed cellulose-based review articles are available covering different fields of research, which includes magnetic sorbents for magnetic solid-phase extraction (Haniffa et al., 2020), lignin incorporated cellulose nanomaterials for various applications (Ewulonu et al., 2019), CNC in bone tissue engineering applications (Murizan et al., 2020), and BC-based composite scaffolds for biomedical applications (Liu et al., 2020). Accordingly, several other cellulose-based review articles are listed in Table 1 for comparison purpose, especially in the field of biomedical applications.

The synthesis of various CSMNs has not been reviewed previously until now. In accordance, this review provides a benchmark guidance on their synthesis and application in biomedical fields of endeavor. As summarized in Scheme 1, this review elaborates typical research and development on the synthesis of CSMNs, and their use in stimulus-responsive drug delivery, cancer therapy, and hyperthermia applications. The review also covers other biomedical applications of CSMNs such as wound healing, MRI, enzyme encapsulation, nucleic acid extraction and tissue engineering applications. The characteristic features of selected CSMNs including, matrix, inorganic materials, shapes, particle size, solvent, synthesis methods and applications are listed in Table 2.

2. Synthesis of cellulose supported magnetic nanohybrids

Cellulose is a linear syndiotactic homopolymer composed of around 1500 D-anhydroglucopyranose rings connected by β-(1–4)-glycosidic bonds. The reasons behind the use of cellulose as a support material for the synthesis of CSMNs can be classified as follows:

(i) cellulose backbone is rich in secondary and primary hydroxyl groups at C2, C3 and C6 positions. Therefore, CSMNs can be created by covalent bonds form between MNPs and cellulose backbone through stable electrostatic interactions under a homogeneous solvent regime (Williams et al., 2019), while cellulose nucleation can be done by introducing MNPs into the cellulose substrate in the heterogeneous solvent system (Tao et al., 2020; Zhang et al., 2019) and;

(ii) hydroxide groups of cellulose backbones not only confer hybridization with the MNPs but easily modified to introduce chemically cross-linkable functional groups through derivatizing reactions.

Table 1
Overview of recent cellulose based review articles in biomedical applications.

Materials	Type of cellulose	Applications	Reference
Polymer composites	BC-nanofibers	Biomedical	(Eslahi et al., 2020)
Magnetic cellulose	Nanocellulose	Enzyme immobilization	(Gennari et al., 2020)
Composite scaffolds	BC-nanofibers	Biomedical	(Liu et al., 2020)
Composite materials	Methylcellulose & cellulose fibers	Biomedical delivery	(Ahmad et al., 2021)
Scaffolds	Nanocellulose	Tissue engineering	(Luo et al., 2019)
Hydrogel	Magnetic natural polymer	Drug delivery	(Liao & Huang, 2020)
Wound dressing materials	Carboxymethyl cellulose	Infection control and wound healing	(Kanikireddy et al., 2020)
Magnetic nanocomposites	Carbohydrate-polymers	Cancer treatment	(Shende & Shah, 2021)
Lignocellulosic-derived NPs	Cellulose nanocrystals & lignin-NPs	Drug delivery	(Wijaya et al., 2021)
Materials	Fibers & nanocrystals	Antibacterial agents	(Ahmad, 2021)
Bone scaffolds	Cellulose nanocrystals	Tissue engineering	(Murizan et al., 2020)

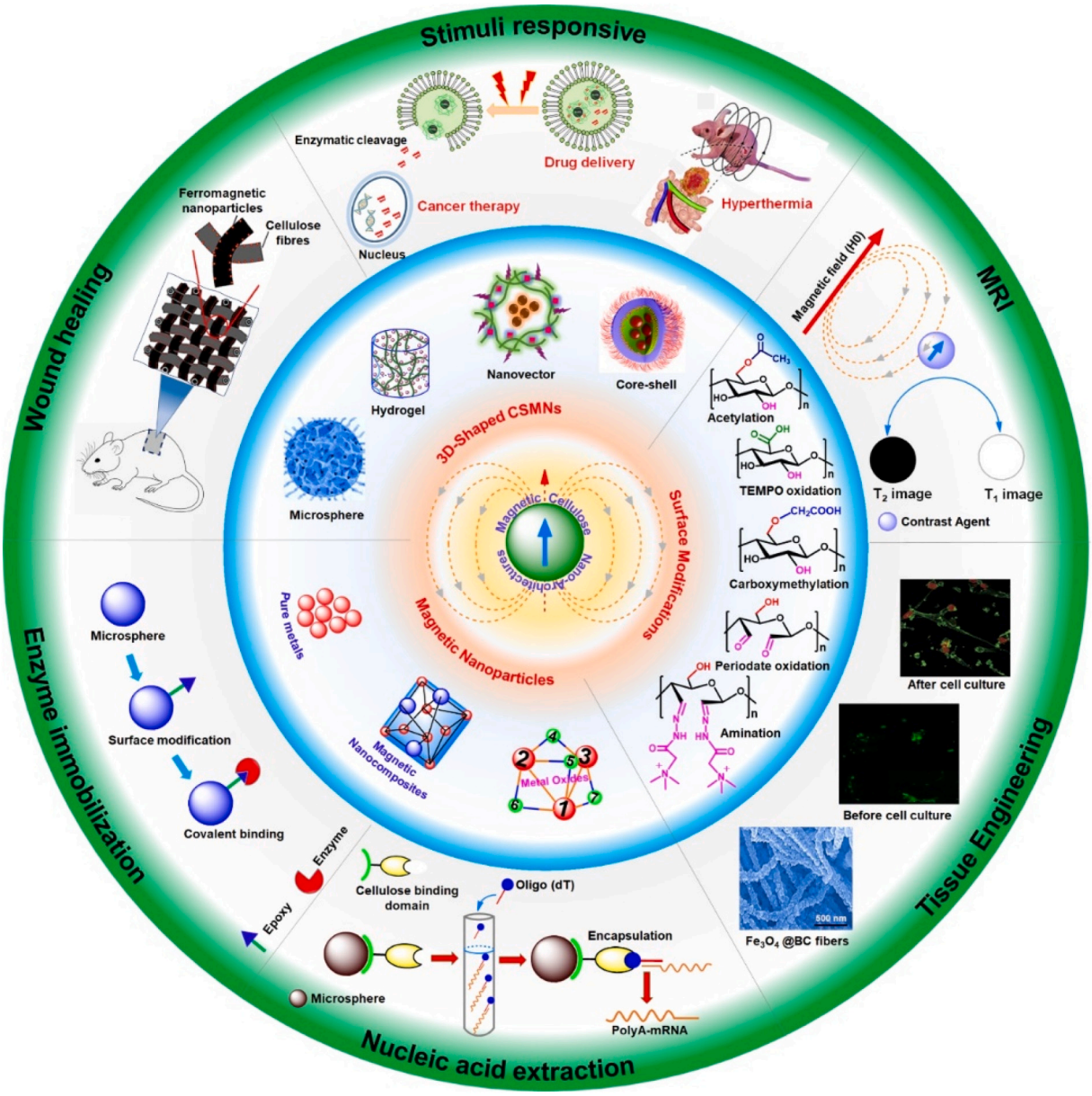

Scheme 1. Schematic illustration of cellulose supported magnetic nanohybrids and their biomedical applications.

Several chemical modifications of cellulose have been reported (Haniffa et al., 2020; Mhd Haniffa et al., 2017), hence covalently functionalized cellulose can be utilized solely or used to crosslink it further with other functional macromolecules to build various CSMNs (Chen et al., 2019; Haniffa et al., 2020; He et al., 2019; Papaparaskeva et al., 2020; Williams et al., 2019). As a result, they can improve the CSMNs' crosslink density, mechanical strength, biofunctionalization (for example, folate), and structural properties, which are effectively simple to hybridize and achieve in either homogeneous or heterogeneous solvent systems. Conversely, the content of MNPs influences the physicomagnetic properties and functional characteristics of CSMNs through magnetic responsiveness, particle size, surface area, magnetic heating, cell variability, cytotoxicity, and so on.

2.1. Preparation of cellulose supported magnetic nanohybrids

In general, synthesis approach of all types of CSMNs is commonly a chemical pathway. However, the designs of different CSMN shapes vary depending on whether the solvent system is homogeneous or heterogeneous. As shown schematically in Fig. 1, the synthesis of CSMNs is comprised of four steps: (1) cellulose solubilization, (2) MNP hybridization, (3) isolation of CSMNs from the reaction mixture, and (4) the phase change (drying) stage.

The solubilization of cellulose is the basic and determinant step in the formation of different CSMNs. It is a mechanism, in which cellulose in a solvent system dissolves to form homogeneity, resulting in Three-dimensional (3D) CSMNs via MNPs encapsulation, or assembles with a heterogeneous surface, resulting in One-and Two-dimensional (1D and 2D) CSMNs through their MNPs nucleation. In general, due to its poor solubility, micro/nanocellulose (MCC, CNC, & CNF) generates heterogeneity with water and contributes to the preparation of 1D and 2D CSMNs. However, cellulose becomes soluble when it:

(i) immersed immediately in the pre-cooled (−5 to −20 °C) mixture of distilled water, urea, and alkali hydroxide at ambient temperature. The presence of urea and alkali hydrates in the mixture has a significant impact on cellulose dissolution at low temperatures. The dissolution power (KOH/urea ≪ NaOH/urea < LiOH/

Table 2
Overview of diverse cellulose supported magnetic nanohybrids' composition, and their synthesis, typical features and applications.

Composition		Synthesis		Typical features		Application	Reference
Matrix	MNPs	Solvents	Technique	Shape	Size		
TEMPO-oxidized microcrystalline cellulose	Fe_3O_4	Deionized water/with an N_2 protective atmosphere	Co-precipitation	Ultra-small magnetic nanoparticle shell	3 nm	Antibacterial	(Biliuta et al., 2017)
Carboxymethyl cellulose	Fe_3O_4 & $CoFe_2O_4$	Water medium in the presence of NH_4OH at 80 ± 2 °C under N_2 atmosphere.	Co-precipitation	Core-shell superparamagnetic nanofluids	7 nm	Oncology and nanomedicine: behaved as nano heaters for killing brain cancer cells in vitro	(Leonel et al., 2019)
Cellulose	$CoFe_2O_4$	Distilled water, ethanol & HCl	Sol-gel	Cubic spinel	< 50 nm	Different application	(Abou Hammad et al., 2019)
Carboxymethyl cellulose	Fe_3O_4	Distilled water	Precipitation	Magnetic spherical hydrogel	10 nm	Drug delivery	(Karzar Jeddi & Mahkam, 2019)
Carboxymethyl cellulose	$Co_{0.25}Cu_{0.25}Mn_{0.5}Fe_2O_4$	Deionized water	Co-precipitation	Nanorods	–	MRI and nanocarrier for drug delivery system	(Abbasi Pour et al., 2017)
Bacterial cellulose membrane	Fe_3O_4	Liquid glucose medium	Biosynthesis (fermentation & incubation)	Smart nanocomposite	6–7 nm	Wound hilling application	(Galateanu et al., 2015)
Bacterial cellulose	Fe_3O_4	Aqueous solution	Immense and precipitation method	Nanocomposite scaffold	N/A	Scaffold for bone tissue engineering	(Torgbo & Sukyai, 2019)
Micro/nano-cellulose dialdehydes	γ-Fe_2O_3	Deionized water	Co-precipitation, periodate oxidation & Schiff-base immobilization	Magnetic solids	N/A	Catalysts	(Tamaddon et al., 2020)
Cellulose	Fe_3O_4	NaOH (7 wt%)/urea aqueous (12 wt %)/water (81 wt%)	Graft	Magnetic hydrogel	2.85–2.88 nm	Controlled drug delivery	(Lin et al., 2019)
Cellulose nanocrystals	Fe_3O_4	Deionized water	Electrostatic self-assembly technique	Glucose oxidase-magnetic cellulose nanocrystals	12.9 ± 6.56 nm	Glucose Detection	(Yee et al., 2019)
Carboxymethyl cellulose	Fe_3O_4	Deionized water	Precipitation & oxidation reaction	Core-shell	N/A	Immobilization prenyltransferases and production of multiple vitamin K2 homologs	(W. Ni et al., 2020)
Cellulose nanocrystals	$CoFe_2O_4$	Water and/or glucose	Evaporation-induced self-assembly (EISA)	Inverse cubic spinel structure with space group Fd-3 m	35–60 nm	Next-generation functional materials	(Lizundia et al., 2017)
Cellulose nanocrystals	Fe_3O_4/Ag	[Bmim]Cl $AgNO_3$ solution (30 ml, 250 mM)	Sol–gel	Aerogel	17/pore size	Medical and environmental	(R. Xiong et al., 2013)
Cellulose nanocrystals	Fe_3O_4	One wt% NaOH solution	In situ Co-precipitation	Nanocomposite films	18–30 nm	Medical diagnostics and tissue engineering	(Dhar et al., 2016)
Polyelectrolytes protamine (pro) and carboxymethyl cellulose	Fe_3O_4	1 M NaCl solution at pH 5	Layer-by-layer (LbL) deposition	Multi-layered nanocapsules	150 ± 20 nm	Drug delivery	(Elumalai et al., 2015)
Cellulose paper	$(Co(NO_3)_26H_2O)$	Deionized water	In situ reduction process using $NaBH_4$ and or H_2 gas	Nanocomposite	2.5 ± 0.7 nm	Antibacterial effect	(Alahmadi et al., 2017)
Hydroxyethylcellulose	Bentonite/magnetite	Deionized water	Solvent casting	Hybrid Materials	30 μm (film thickness)	Antifungal activity	(Alekseeva et al., 2017)
Nano-fibrillated cellulose	Fe_3O_4@TiO_2	Deionized water	Sol-gel process	Nanocomposite	5–8 nm	Wastewater treatment and biomedical engineering	(An et al., 2017)
Bacterial Cellulose Pellicles	Fe_3O_4	Deionized water	In situ precipitation	Magnetic hydrogel	49.81 ± 20.77 nm	Tissue engineering applications (vascular grafts, capture and improve cell retention of other types of applications)	(Arias et al., 2018)
PVA and PCMC	Fe_3O_4		Freeze-thaw cycles (freezing	Hydrogel	N/A	Drug delivery system	(Dai et al., 2019)

(*continued on next page*)

Table 2 (*continued*)

Composition		Synthesis		Typical features		Application	Reference
Matrix	MNPs	Solvents	Technique	Shape	Size		
		Ionic liquid 1-butyl-3-methylimidazolium chloride (BmimCl)	at −20 °C for 8 h and thawing at RT for 4 h) and Co-precipitation				
Reduced graphite oxide	$NiCl_2{\cdot}6H_2O$	Deionized water	Grafting and doping techniques	Nanocomposite (ferromagnetic material)	10–60 nm	Biosensor and biocatalyst	(Dhahri et al., 2018)
Sisal cellulose	Fe_3O_4	LiCl/DMAc (*N*,*N*-dimethylacetamide) solvent	Solvent casting	Magnetic hybrid films	5.1 ± 0.5 nm	Biomedical miniaturized electronic devices, and advanced catalysis applications	(Furlan et al., 2019)
Microcrystalline cellulose	Fe_3O_4	Solution with NaOH/urea/H_2O (weight ratio, 7:12:81)	Refluxing, surface modification Covalent attachment	Core-shell structured magnetic cellulose microsphere	100–650 nm	Enzyme immobilization	(Xue et al., 2019)

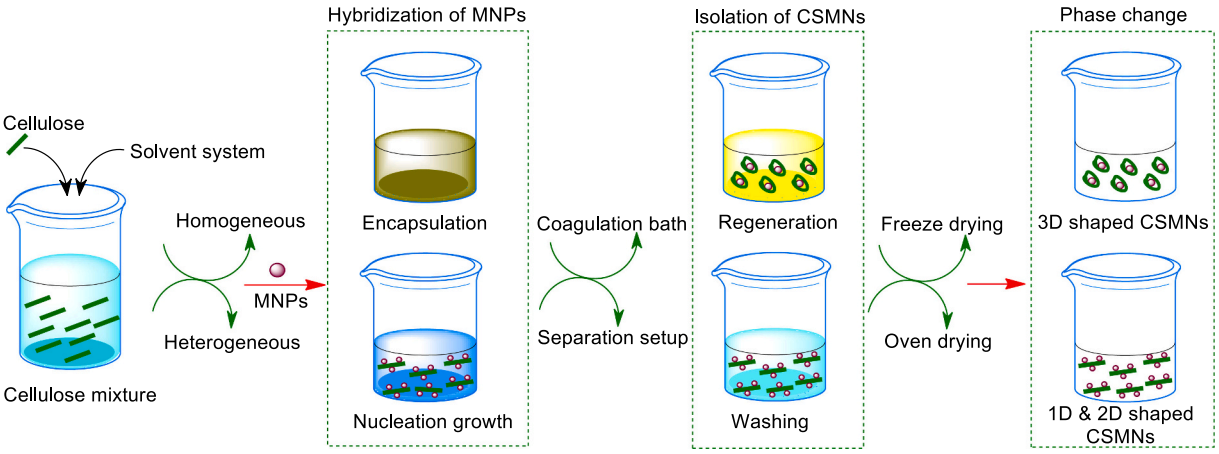

Fig. 1. Typical schematic of the preparation of CSMNs through four basic steps, consisting of cellulose solubilization, MNPs hybridization, CSMNs isolation, and phase change methods.

urea) of this type of non-derivatizing solvent system is related to the temperature of the solvent, the amount of urea, and the hydroxide concentration of the alkaline species (Cai & Zhang, 2005) and;

(ii) undergoes selective surface modification such as carboxylation, methylation, ethylation, amination, and so on. As a result, as formed homogeneous cellulose mixtures are used to encapsulate MNPs.

By contrast, due to its poor solubility, BC provides an excellent fibrous aspect ratio and surface reactivity, which allows absorbing a large number of MNPs in a heterogeneous manner in a water medium (Haniffa et al., 2020). It is because, BC extremely fine fibril nature and lack of other biopolymers usually associated with plant celluloses, such as hemicellulose and lignin (Schlufter et al., 2006). However, ionic liquids (ILs) based solvent offers a promising pathway to overcome this limitation (Haniffa et al., 2020). In particular, 1-N-butyl-3-methylimidazolium chloride ($[C4mim]^+Cl^-$) has been reported for selective surface functionalization of BC (degree of polymerization (DP) up to 6500) under the homogeneous reaction conditions. It is also recommended as a non-derivatizing solvent for the homogeneous surface functionalization of plant cellulose with a DP up to 12,000 (Schlufter et al., 2006). In this context, washing and regeneration methods are used to separate various-CSMNs from as-prepared MNPs-cellulose mixtures.

2.2. Shapes of cellulose supported magnetic nanohybrids

Typically, 1D and 2D CSMNs includes fibers (Ghosh et al., 2019; Hou et al., 2016), nanorods (Abbasi Pour et al., 2017; Chen et al., 2014), and film (Dhar et al., 2016; Furlan et al., 2019; Li et al., 2017; Liu et al., 2011; Turyanska et al., 2012; Yang et al., 2020), can be generated through washing and oven drying, while freeze-dried 3D CSMNs such as magnetic hydrogel, micro-spheres, enzyme-bound nano-spheres, nano-carriers, metal-organic framework, actuators, core-shell nano-conjugates, scaffold and so on, are generated through regeneration and phase changing steps (Fig. 1). Apart from the oven and freeze-drying methods, separation based on EMF has also been used on some occasions to collect the CSMNs from the reaction mixture (Yee et al., 2019).

An effective Fe_3O_4 immobilization was performed on CNCs nanorod (CNC@Fe_3O_4) with an aspect ratio of 20 in the heterogeneous CNC/water/PDDA mixture of cellulose. To improve its thermal stability and to facilitate more —OH groups on their surface, as-prepared polyvinylpyrrolidone-capped nanorod is coated with SiO_2. The β-cyclodextrin (β-CD) grafting of this SiO_2 coated nanorod has not only speed up the adsorption of pharmaceutical residues compared to without β-CD grafted nanorod, but also transformed its structure into a core-shell (Chen et al., 2014). Limaye and his colleagues developed spinel structure cobalt ferrite (COF)@CMC nanofiber-based bio-composite free-standing films through an in-situ synthesis of COF NPs in CMC-nanofiber matrix (Limaye et al., 2019). They also introduced

COF@CMC-NF-based biocomposite 3D patterns for the very first time with lateral dimensions of ~1.2 μm. By contrast, CMC/water/NaOH-based homogeneous cellulose mixture has been proven an efficient Fe_3O_4 encapsulation, where freeze-dried spherical CSMN (Fe_3O_4@CMC) exhibit lower binding energy to immobilized prenyltransferase NovQ. In addition, Wang and Co-workers reported the single-magnetic-responsive beam-, accordion- and star-shaped actuators made of Fe_3O_4 and cellulose paper (Wang et al., 2018). They actuated the actuators with a NdFeB magnet to study their actuation performance. The different types of hybrid magnetic particles used in diversified applications are listed in Table S1.

The hydrogel is an astonishing material similar to the body tissue by water uptake capacity, nearly 70–99%, which can provide biocompatibility and encapsulation potential of hydrophilic drugs (Taghizadeh et al., 2019). Besides, divalent metal ions such as Ca^{2+}, Sr^{2+}, Zn^{2+}, Cu^{2+}, Ba^{2+}, and so on can be used for the designs of single-and multi-layered beads via the chelation technique (Wang et al., 2011). However, compared to single-layered beads, multi-layered beads are a well-controlled drug delivery system because of their diffusion barrier to slow rapid drug release (Elisseeff, 2008). In this regard, β-CD grafted cellulose-based magnetic hydrogel-beads have been reported for remotely controlled drug releasing application (Lin et al., 2019). The beads were fabricated via a facile extrusion technique in a calcium chloride coagulation bath. Electrostatic adsorption and hydrogen bonding enabled the Fe_3O_4 NPs to occupy and attach to the β-CD grafted cellulose of the beads. The drug loading activities of the beads are controlled by β-CD and Fe_3O_4 NPs through their host-guest complex formation and pore size respectively. The controlling attributes of β-CD and Fe_3O_4 NPs are given as follows:

i) The formation of a host-guest complex between the cavities of β-CD and the drug molecules increases drug loading efficiency as compared to β-CD free magnetic beads.
ii) Fe_3O_4 NPs occupy the hydroxyl groups of the β-CD grafted cellulose backbone, reducing the pore size of the beads and thereby lowering drug loading volumes.

Recently, polyporous structured magnetic cellulose beads have been stated as an efficient and recyclable catalytic support to immobilize the *Candida Antarctica* lipase (CAL) (Zhang, Liu, et al., 2020). The CAL has been immobilized with PSMCBs through glutaraldehyde, which has been used as a crosslinker to covalently link CAL to various types of amine terminated PSMCBs. Besides, the carbodiimide-coupling technique was used to make a covalent link between glucose oxidase (GOx) and magnetic CNC-COOH (Yee et al., 2019). Hence, the immobilization of GOx is achieved via nucleophilic attack of their $-NH_2$ groups on the carbonyl carbon of —COOH groups present in the magnetic CNC surface (Malakootikhah et al., 2017). The MNPs (Fe_3O_4 and/or γ-Fe_2O_3) of this CSMN have attached with CNC-COOH through electrostatic self-assembly technique. As prepared GOx immobilized CSMN, utilized for glucose detection in which GOx is used as an enzyme to catalyze the glucose oxidation (Yee et al., 2019).

As shown in Fig. S1, core-shell structured CSMN nanocarrier has been reported for pH-triggered DOX release, in which double layers of polysaccharide shells have been created over Fe_3O_4 NPs using dialdehyde salep (DAS) and polyethylene glycol (PEG) functionalized CMC (CPEG) (Hosseini et al., 2020). The strategy of this nanocarrier creation is quite interesting, in which authors used Zeta potential to confirm the development of the double layers. The CPEG layer has proven to have the most important functions in making Fe_3O_4@DAS@DOX@CPEG nanocarrier more efficient, including:

(i) CPEG has played a key role in reducing the release rate of DOX, therefore reduces the negative side effects of drugs in normal tissues (pH 7.4) and has proven to be a potential candidate for in vivo cancer therapy;
(ii) biocompatibility of the CPEG towards normal cells attributed to the nanocarrier can be considered for in vivo use;
(iii) the CPEG promotes the cellular uptake of nanocarrier due to the presence of PEG chains through endocytosis mechanism and;
(iv) hemocompatibility of the CPEG can prevent the release of hemoglobin from the membrane of the erythrocytes into the plasma.

Interestingly, Li and Co-workers developed a metal-organic framework (MOF) anchored cellulose acetate membrane for enzyme encapsulation (Li et al., 2021). Authors used zeolitic imidazolate framework-8 (ZIF-8) as MOF for this encapsulation, which generally consists of zinc metal and 2-methylimidazole ligands. Cao and his colleagues prepared core-shell CSMN and enzyme encapsulated ZIF-8 based nanocomposite in an earlier study, in which homogenous cellulose mixture based on MCC/NaOH/urea used for CSMN synthesis (Cao et al., 2017). The MOF has been targeted for these kinds of nanohybrids because: (1) it has attracted extensive attention in sensing and drug delivery; (2) of its merits of high BET surface area and porosity; (3) of its exoskeleton structure used to protect vulnerable biological macromolecules such as enzymes (GOx, laccase, horseradish peroxidase and so on), DNA, and viruses and; (4) of its excellent physiochemical characteristics and easy recovery under magnetic field.

Torgbo and Co-workers developed functional bone tissues like scaffold recently (Torgbo & Sukyai, 2019). They used nano-HA to coat a Fe_3O_4 embedded BC membrane using an ultrasonic irradiation technique in deionized water, resulting in an osteo-mimetic architecture scaffold. The advantages of this type of scaffold development are as follows: (1) MNPs are easily recognized by bone tissue via mechano-electrical conversion in the scaffold; (2) presence of calcium phosphate bioceramics improves the cellular behavior of the scaffold by encouraging high proliferation and faster differentiation of osteoblasts cells, stimulating new bone tissue formation, growth, and bioactivity and; (3) HA coating with Fe_3O_4 enhances the solubility of the composites in physiological solutions more than HA alone.

Another study has reported a core-shell nanoconjugate consisting of CMC and MNPs in a homogeneous mixture of CMC/water/NH_4OH (Leonel et al., 2019). Authors used CMC as a ligand to encapsulate the respective Fe_3O_4 and Cobalt-doped Fe_3O_4 NPs (CMC@$Co_xFe_{3-x}O_4$), which helped to produce a colloidal aqueous solution without the proper subsequent dispersion of these NPs in polymer medium. As a result, a single-step one-pot process was used to encapsulate the MNPs and regenerated them in a reflux setup containing their colloidal aqueous solution.

3. Physicomagnetic properties of cellulose supported magnetic nanohybrids

The magnetic behavior of CSMN is constrained based on its magnetic parameters, such as magnetization, remanence, and coerciveness, which are influenced by the physical properties of the nanomaterials of CSMN, essentially MNPs, and the micro/nano-cellulose. It is known that the volume of MNPs has also created an impact on the mechanical properties of the CSMNs. For instance, the recent report of a hybrid film based on sisal cellulose@Fe_3O_4 (Furlan et al., 2019) was found that the integration of Fe_3O_4 into the cellulose matrix; (1) decrease the stiffness as well as the resistance against the deformation of the hybrid film and; (2) decrease the tensile strength. However, the impact of physical properties such as MNP size and composition, cellulose forms, and CSMN shapes on the magnetic behavior of CSMNs has been addressed in this section through their magnetic parameters.

In general, superparamagnetism is preferred over ferromagnetism in biomedical applications due to its high magnetic moment and giant paramagnetic nature (Cardoso et al., 2018). Because the CSMN with superparamagnetic performance exhibits rapid response to EMF with negligible remanence and coercivity (H_C) at RT (Cardoso et al., 2018;

Hao et al., 2010) (Fig. 2). In furtherance, superparamagnetic NPs dissipate heat in magnetic fluid hyperthermia by Néelian and Brownian relaxation in the presence of an alternating magnetic field (Ng & Kumar, 2017). Overall, the presence of superparamagnetic property in CSMN could be possible due to the weak interaction among individual MNPs via covalent bonding with the cellulose substrates. For instance, this phenomenon has been demonstrated by $CoFe_2O_4$ NPs nucleation on a diamagnetic carboxymethyl CNF surface, which showed a linear increase in magnetization with respect to the EMF (Williams et al., 2019). In this regard, the subsections are briefing the impact of various MNPs and cellulose substrates on the physicomagnetic properties of the CSMNs. The different physicomagnetic properties associated with vibrating magnetometer-based sample effects, as well as the Brunauer-Emmett-Teller (BET) surface area of different CSMNs, are shown in Table 3.

3.1. Fe_3O_4 NPs based cellulosic magnetic nanohybrids

In general, Fe_3O_4 NPs become superparamagnetic at RT when their size is less than about 15 nm. The CNC nanorods loaded with Fe_3O_4 NPs, on the other hand, have shown superparamagnetic properties, with saturation magnetization (M_s) of ~50.5 emu/g and infinitesimal H_C without any diverse hysteresis loop at RT (Dhar et al., 2016). It indicates that the integration of Fe_3O_4 NPs with particles of size 18–30 nm into the CNC nanorods has not disturbed its ferromagnetic nature but has changed the M_s relative to Fe_3O_4 NPs (92 emu/g) in bulk. Although, integration of Fe_3O_4 NPs enhanced CNC nanorod properties such as dispersion, alignment (parallel and perpendicular directions), and overall crystallinity in the PLA matrix, which subsequently improved the mechanical, thermal and electrical properties of the resulting PLA-CNC@Fe_3O_4 film (Dhar et al., 2016). However, coating with diamagnetic SiO_2 over CNC@Fe_3O_4 nanorod significantly reduced its M_s value from 14.0 to 10.3 to 7.0 to 5.0 emu/g, with rising shell thicknesses of 5.9, 8.0, 10.9, and 14.1 nm respectively (Chen et al., 2014).

By contrast, a similar study observed an increasing trend in M_s from 13.4 to 18.9 emu/g when the Fe_3O_4 content increased with no obvious remanence and H_C for cellulose@Fe_3O_4/β-CD-hydrogel beads (Lin et al., 2019). However, cellulose@Fe_3O_4-hydrogel beads were exhibited 9.34 emu/g of M_s in another study for a fixed amount of Fe_3O_4 NPs (B. Li, Zhang, et al., 2020). In both cases, cellulose has been used as a substrate instead of CNC, and it has been dissolved in the respective solvent system NaOH/urea/water (7:12:81 (*w*/w)) and [BMIM]Cl ionic liquid. Hence, the cellulose associated beads offered a higher surface area, which allows them to encapsulate a large amount of Fe_3O_4 NPs in homogeneous solvent mixture.

The introduction of HA on BC@Fe_3O_4-membrane has reduced its M_s value from 15.84 to 3.94 emu/g at ±10 k Oe (Torgbo & Sukyai, 2019). As formed trabecular/cancellous bone-like BC@Fe_3O_4-HA structure has also exhibited 81.1% of porosity together with respective compressive strength and Young's modulus of 9.87 MPa and 1.85 GPa. It was suggested that the tremendous decrease in M_s could be attributed to: (1) the oscillation effect of ultrasonic radiation during the synthesis of HA and;

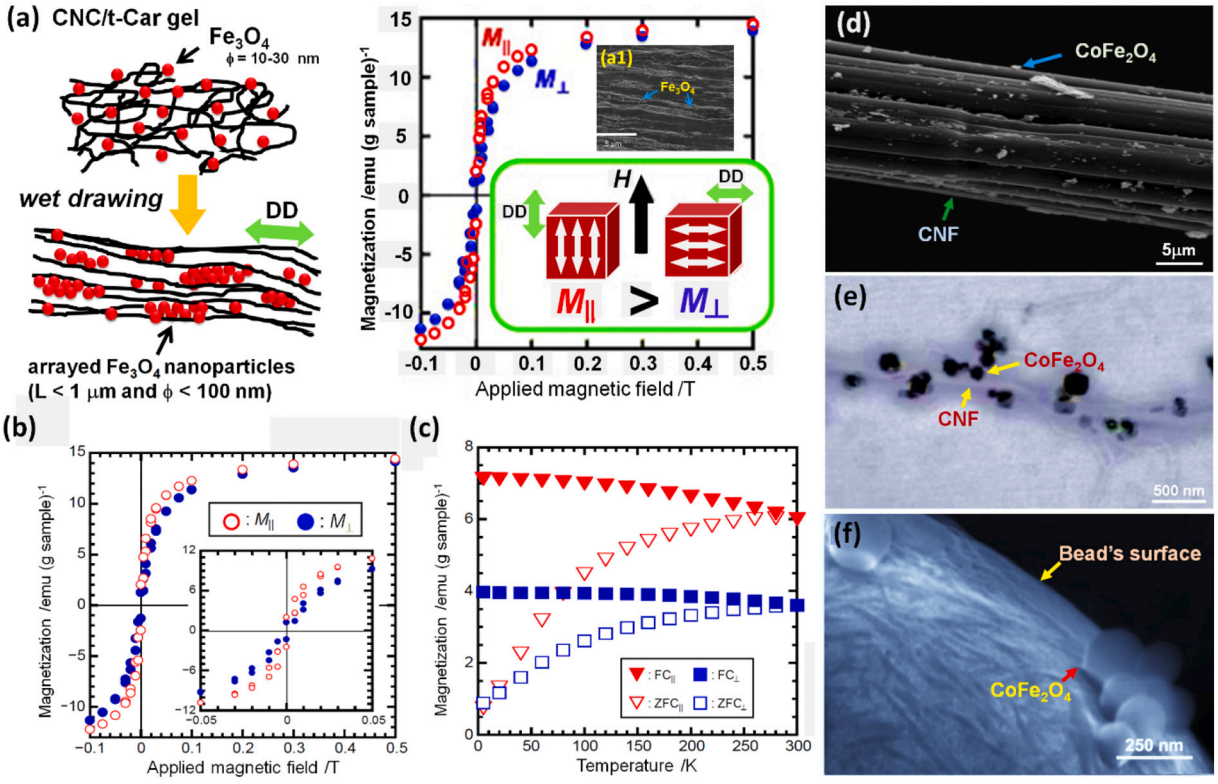

Fig. 2. a), The graphic illustration that models the oriented aggregates of Fe_3O_4 NPs distributed in the CNC/i-carrageenan (*ι*-Car) gelatinous composites, drawn film and magnetometry characterization with two sets draw direction (DD), parallel (||: red mark) and perpendicular (⊥: blue mark) to the applied field; (a1) FESEM image of the fracture surface morphology of the drawn film; b) Magnetization vs applied field plots at 298 K, depicted in a narrow range of the field strength and; c) Temperature dependence of magnetization, exhibited with a field strength of 0.01 T in zero-field-cooled (ZFC: open symbol) and field-cooled (solid symbol) conditions Adapted and reprinted from Yoshitake et al. (2016) with proper permission from Elsevier, (Yoshitake et al., 2016). $CoFe_2O_4$ NPs immobilized on functionalized cellulose fiber. d), SEM image at a magnification of 4300× Adapted and reprinted from Williams et al. (2019) with proper permission from American Chemical Society, (Williams et al., 2019). e), TEM image, decorated with 96.5 wt% $CoFe_2O_4$ NPs showing that all particles are associated with fibers Adapted and reprinted from Galland et al. (2014) with proper permission from American Chemical Society, (Galland et al., 2014). f), SEM image of polystyrene microbeads encapsulated in a CNC shell containing ex-situ synthesized $CoFe_2O_4$ NPs inside the polystyrene core Adapted and reprinted from Nypelö et al. (2014) with proper permission from American Chemical Society, (Nypelö et al., 2014).

Table 3
Physicomagnetic properties of selected cellulose supported magnetic nanohybrids and their magnetism and applications.

Cellulose supported magnetic nanohybrids	Physical properties	Magnetic properties			Magnetism	Application	Reference
		M_s/ emu/g	M_r/ emu/ g	H_C/Oe			
6-Carboxy Cellulose@Fe_3O_4	Shape: Core-shell; Size: 129 nm; d_h: 719 nm; Stability (ξ): −50 mV	7.70	–	–	Superparamagnetic	Contrast agent (MRI)	(Biliuta et al., 2017)
Polyaniline/Cellulose/$CoFe_2O_4$	Shape: Nanocomposite thick film; Size: 50 nm ($CoFe_2O_4$); Conductivity: 3.5×10^{-3} S/cm.	3.70	1.56	933.00	Ferromagnetic	Antimicrobial	(Abou Hammad et al., 2019)
CNC@Fe_3O_4@Chitosan	Shape: Rod; Size: width 50 nm & length 600 nm	10.10	–	–	Superparamagnetic	Enzyme	(Cao et al., 2015)
BC–Fe_3O_4 (BC: Bacterial cellulose)	Shape: Nanocomposite scaffold; Porosity: 82.9%	15.84	–	–	Superparamagnetic	Scaffold	(Torgbo & Sukyai, 2019)
BC–Fe_3O_4-HA (HA: Hydroxyapatite)	Shape: Nanocomposite scaffold; Porosity: 81.1%	3.94	0.17	7.12	Superparamagnetic	Scaffold	(Torgbo & Sukyai, 2019)
CNF@Fe_3O_4/Ag	Shape: Aerogel; Size: ~18 nm (Fe_3O_4) & ~23 nm (Ag); BET-SA: 61.00 m^2/g; Pore diameter: 17 nm	64.50	0.70	8.90	Superparamagnetic	Antibacterial	(R. Xiong et al., 2013)
CNF@Fe_3O_4/Ag	Shape: Film; Size: ~18 nm (Fe_3O_4) & ~23 nm (Ag); BET-SA: 0.12 m^2/g; Max pore diameter 20 nm at pore volume: 1.1×10^{-4} cm^3/nm/g	52.70	0.90	11.80	Superparamagnetic	Antibacterial	
Hydroxyethyl cellulose@bentonite-Fe_3O_4	Shape: Hybrid film; Film thickness: 30 μm; Average particle diameter: 6.3 μm; BET-SA: 11.46 m^2/g; Pore diameter: 15.35 ± 1.55 nm	5.96	1.03	68.80	Ferromagnetic	Antifungal	(Alekseeva et al., 2017)
BC@Fe_3O_4	Shape: BC's fibrils; Size: 49.81 ± 20.77 nm (diameter of fibril@Fe_3O_4)	10.00	–	–	No hysteresis loops formed	Tissue engineering	(Arias et al., 2018)
Pineapple-peel-Cellulose/ PVA@regenerated nanocellulose@Fe_2O_3	Shape: Hydrogel; Aspect ratio: 330/25 (regenerated nanocellulose used for reinforcement); Swelling kinetics: $K = 0.0891$ & Qe, exp = 28.27 (g/g)	18.79	–	–	Superparamagnetic	Drug delivery	(Dai et al., 2019)
Cellulose-BTCA@Fe_3O_4	Shape: Core-shell; Size: 10 ~ 15 nm (thickness of the cellulose shell) & 450 nm (whole structure)	34.90	Negligible remanence and coercivity-		Superparamagnetic	Enzyme	(Xue et al., 2019)
Acidic/nanocellulose@Fe_3O_4	Shape: Magnetic nanocellulose particles; BET-SA: 15.00 m^2/g; Pore diameter: 11 nm at pore volume: 2.71×10^{-3} cm^3/nm/g; load ca	18.60	–	4.00	Superparamagnetic	Enzyme	(A. Gennari et al., 2019)
Basic/nanocellulose@Fe_3O_4	Shape: Magnetic nanocellulose particles; BET-SA: 16.00 m^2/g; Pore diameter: 8 nm at pore volume: 1.6×10^{-3} cm^3/nm/g	14.00	–	–	Superparamagnetic	Enzyme	(A. Gennari et al., 2019)

BET = Brunauer-Emmett-Teller; SA = surface area; M_s = saturation magnetization magnetization; M_r = remanence; H_C = coercivity; d_h: hydrodynamic diameter; ξ: zeta potential; BTCA = 1,2,3,4-butanetetracarboxylic acid; Qe, exp = Schott's second-order kinetic model; K = Fickian diffusion model.

(2) the cladding on the matrix of Fe_3O_4 NPs by HA creates the layer of surface spin disorder that leads to diamagnetic shell formation and it leads to a subsequent reduction in the magnetic moment at the interface. On the other hand, the shielding effects of HA lead to decrease remanent magnetization (M_r) from 0.89 emu/g to 0.17 emu/g and the H_C to 7.12 Oe. The negligible M_r and minimal H_C have confirmed the scaffold's superparamagnetic characteristic and become favorable for guided bone tissue engineering application with or without EMF (Torgbo & Sukyai, 2019). In addition, the M_s value of the Cu(II) chelated cellulose/ magnetic-HA hybrid beads (MHAB) was found to be still strong enough to separate the Histidine-Rich proteins from the solution with the 20s even after their reduction from 64.4 (Fe_3O_4) to 29.2 (MHAB) emu/g (Du et al., 2018).

In contrast, Cu(II) chelated metal affinity adsorbent (Graphene-oxide@Fe_3O_4/CMC@Iminodiacetic acid (IDA)-Cu(II)) has been used to isolate the histidine-rich proteins, which shown lower M_s of 16 emu/g than bulk Fe_3O_4 due to the presence of Cu(II) coordination (Liang et al., 2019). However, without the CMC support Graphene-oxide@Fe_3O_4 (M_s of 18.5 emu/g) showed a fully reversible magnetization curve with superparamagnetic nature, without hysteresis loop, negligible remanence, and coerciveness (Liang et al., 2019). It is clear that CMC has a significant impact on the hysteresis loop of the CSMN in both situations such as before (Ms of 16.5 emu/g) and after immobilization of Cu(II) (M_s of 16 emu/g) compared to Graphene-oxide@Fe_3O_4. Moreover, the encapsulation of core-shell CSMN (Cellu@Fe_3O_4) into the ZIF-8 exoskeleton declined the M_s values of Cellu@Fe_3O_4 to 4.9 emu/g from 12.8 emu/g (Cao et al., 2017). Similarly, the actuator based on paper@Fe_3O_4 exhibited M_s of 33.5 emu/g as compared to its MNPs counterpart, which was 63.1 emu/g (Wang et al., 2018). This study observed low magnetic hysteresis due to large bending deformation that exceeds the elastic deformation limit of the actuator. Therefore, causing irreversible deformation that led to reversible flexural deformation of the actuator. All of the CSMNs mentioned above, including nanorod, film, hydrogel bead, core-shell, and actuator, showed different M_s values for Fe_3O_4 NPs, demonstrating that cellulose forms, CSMN types, and CSMN synthesis strategies all had an impact on M_s.

3.2. $CoFe_2O_4$ NPs based cellulosic magnetic nanohybrids

The $CoFe_2O_4$ NPs are highly preferred due to excellent chemical stability, tunable H_C, high cubic magneto-crystalline anisotropy caused by spin-orbit contributions, moderate saturation magnetization, unique light-induced H_C changes, good electromagnetic properties, and mechanical hardness (Williams et al., 2019). Superparamagnetic NPs are known as single ferromagnetic domains in which all spins are closely connected. $CoFe_2O_4$ is a ferromagnetic NP (FMNP) and this kind of FMNPs is capable enough to produce temperature-dependent magnetic properties. Indeed, $CoFe_2O_4$ is an inverse spinel, with the octahedral sites are equally occupied by divalent (Co^{2+}) and trivalent ions (Fe^{3+}) whereas trivalent ion (Fe^{3+}) occupying all tetrahedral sites. The M_s of $CoFe_2O_4$ has found to be almost the same level when increasing the temperature in which the hysteresis loop becomes wider as shown in Fig. S2(a) (Williams et al., 2019). In furtherance, the abrupt change in the M_s value was observed in the low field part of hysteresis at 100 K and

4 K temperatures (Chybczyńska et al., 2019).

The FMNP's properties are very sensitive to temperature changes, they can respond to changes in temperature relative to their Curie temperature (T_C) like other magnets. T_C is a temperature, in which: (1) materials lose their permanent magnetic properties; (2) FMNPs are ordered at below T_C and disordered at above T_C, and; (3) M_s approached to zero. In this context, Williams and his colleagues developed a smart wound dressing based on $CoFe_2O_4$ integrated cellulose fibers (Fig. 2(d)) to introduce the wireless wound-healing monitoring technology (Williams et al., 2019). The magnetic fibers revealed ferromagnetism with M_s of 84.5 emu/g for the maximum $CoFe_2O_4$ NPs' content by volume in the fiber matter. The purpose of this research was to use temperature as a biomarker for their ability to communicate wirelessly.

Wan and his colleagues developed a ferromagnetic $CoFe_2O_4$ integrated cellulose aerogel (Wan & Li, 2015). As illustrated in Fig. S2(b), it has a M_s value of 8.6 emu/g at 300 K. The M_s value of the aerogel was found to be much lower than the M_s value of the $CoFe_2O_4$ component itself (52.1 emu/g) and the $CoFe_2O_4$ bulk (80.8 emu/g). It was accepted that this could be due to the comparatively smaller particle size of the $CoFe_2O_4$ resulting from the existence of the hierarchical porous aerogel matrix, which induces an increase in surface effects. The surface layer on the other hand does not have an impact on the M_s value, but it is remarkable to reduce M_s by reducing the particle size. Also, it can have a proportional effect on the surface charge based on its hydrodynamic diameter (d_h), for instance, around 20% surface charge reduction was reported for a relatively higher d_h value of CMC@$Co_xFe_{3-x}O_4$ nanoconjugate compared to analogous Fe_3O_4 NPs (Leonel et al., 2019). It is due to the polymer chain of CMC and their carboxylate groups that facilitate minimizing the electrostatic repulsions (i.e., free energy), affecting the overall balance charges in the water medium.

Besides, electron paramagnetic resonance spectroscopy revealed that CMC@$Co_xFe_{3-x}O_4$ has a much stronger anisotropic temperature dependence. Blocking temperature (T_B) and magnetic hardness properties of Fe_3O_4 NPs are affected by the introduction of CMC-based surface layer and cobalt doping. Therefore, uncoated Fe_3O_4 NPs and undoped CMC@Fe_3O_4 nanoconjugates had TB = 290 K and 105 K, respectively, while CMC@$Co_xFe_{3-x}O_4$ nanoconjugates had TB = 190 K, indicating that the thermal energy of the Fe_3O_4 NPs is reduced, and the magnetic moments are blocked. Strong hysteresis and higher H_C field at 77 K evidenced magnetically harder behavior of CMC@$Co_xFe_{3-x}O_4$, whereas due to their small magnetic hysteresis, CMC@Fe_3O_4 nanoconjugate referred to as magnetically soft at 77 K (Leonel et al., 2019).

It should be noted that the addition of NPs usually renders the composite film fragile and thus produces functional cracks in the film. Therefore, to get the crack-free film or to reduce the brittleness of the CSMN composite film, the third phase can be added to the system. In this context, glucose has employed as the third phase to the CNC/$CoFe_2O_4$ composite to get the crack-free film and to enhance the M_s (Lizundia et al., 2017). It was found that the glucose-incorporated composite film (CNC/glucose/$CoFe_2O_4$) showed maximum M_s of 12.96 emu/g, while the glucose-free composite film (CNC/$CoFe_2O_4$) showed only 8.47 emu/g for the same amount of 20 wt% of the $CoFe_2O_4$ NPs as shown in Fig. S2 (c). As a result, glucose has not only been used as a contributor to crack-free film manufacturing but also as a M_s enhancer, which is possible by offering a large surface area for the integration of agglomerate-free $CoFe_2O_4$ NPs (Lizundia et al., 2017).

Interestingly, Chybczyńska and Co-workers reported hybrid thin films containing MCC and CNC (1 wt%) as a filler along with $CoFe_2O_4$ (60 wt%) separately in the chitosan matrix (Chybczyńska et al., 2019). The formed film showed a temperature dependence (between 300 K and 4 K) on hysteresis (M-H loop), especially at low temperatures as shown in Fig. S2(d). The H_C value of the $CoFe_2O_4$@chitosan has increased compared to the hybrid thin film without MCC, and it was even higher than in the pure $CoFe_2O_4$ (Chybczyńska et al., 2019). However, the wasp-like hysteresis of the films has disappeared after the successful incorporation of MCC or CNC. The wasp-like hysteresis can be caused by: (1) combination effect: magnetic anisotropy and magnetic dipolar interaction; (2) a mixture of a single-domain phase (high H_C) and a multi-domain phase (low H_C) and; (3) change in the ion occupation number between A-sites (tetrahedral) and B-sites (octahedral).

It was observed that the film with MCC and CNC exhibited respective M_s values of 22 emu/g and 16 emu/g. Higher M_s of MCC is attributed due to its aspect ratio, in which MCC separates the spinel grains for larger distances than CNC. Furthermore, the MCC incorporated film had a higher H_C of 0.2033 at 300 K than the CNC containing film, which had 0.1696 at the same temperature, and both films had the same H_C at 4 K.

3.3. $MnFe_2O_4$ NPs based cellulosic magnetic nanohybrids

The particle size of $MnFe_2O_4$ smaller than the related critical single-domain size (< 20 nm), leading them to exhibit superparamagnetic behavior (Vamvakidis et al., 2013). However, it was observed that the M_s values increased significantly as the overall concentration of $FeCl_3$/$MnCl_2$ increased, showing the adaptability of the magnetic properties. On one hand, the bulk $MnFe_2O_4$ has a spinel-type collinear ferrimagnetic spin structure compared to a small particle size, which shows lattice expansion. In brief, at bulk sample, Mn ions exist as divalent (Mn^{2+}: 3d5, moment: 5 μB), trivalent (Mn^{3+}: $3d^4$, moment: 4 μB) or tetravalent (Mn^{4+}: $3d^3$, moment: 3 μB), in NPs samples. Hence, the lattice parameter would expectedly be decreased with the decrease in particle size without any changes in the valence state of the Mn ions. Consequently, on the other hand, the core-shell model is associated with the decrease of the magnetic moment in the NPs.

Owing to its high surface energy, $MnFe_2O_4$ particles tend to aggregate easily, which leads to an impact on their dispersion stability. This phenomenon is illustrated by a positively charged cellulose activated carbon (CAC)@$MnFe_2O_4$ hybrid, which was generated using a simple one-pot solvothermal method that involved immobilizing $MnFe_2O_4$ NPs on the surface of CAC (Chen et al., 2019). The hybrid particles showed similar dispersion stability closer to the CAC and also, higher than $MnFe_2O_4$ due to their reduced surface energy after $MnFe_2O_4$ NPs being loaded onto the CAC. This implies that the uniform distribution and immobilization of the $MnFe_2O_4$ NPs along the CAC surface has reduced their surface energy. Consequently, the surface defect of $MnFe_2O_4$ reduced the bulk of M_s 82 to ~60 emu/g (Aguilar et al., 2019). However, when CAC used as a template for $MnFe_2O_4$ NPs nucleation (CAC@$MnFe_2O_4$), the M_s has dropped further to the lowest value of 17.7 emu/g (Chen et al., 2019). The lowest M_s value of 5.56 emu/g has also been reported for a catalyst based on CNC@$MnFe_2O_4$ than those of bare $MnFe_2O_4$ (64.99 emu/g) NPs (Zhan et al., 2018). The overall M_s of this catalyst has decreased as the EMF increased because: (1) at low magnetic fields, $MnFe_2O_4$ exhibited dominant ferromagnetism (Zhan et al., 2018) and; (2) the diamagnetic property of substrate or template (CNC, CAC, etc.) is dominated at higher magnetic fields (Aguilar et al., 2019). Overall, MNPs with higher M_s and negligible H_C are permissible for biomedical applications, while high H_C leads to higher resistance to CSMN demagnetization, which is best for use as a recyclable catalyst. Overall, cellulose and its forms, and also MNPs and their inherent properties, have proved their significance in the physicomagnetic properties of CSMNs.

4. Biomedical applications

To underscore the systemic roles of CSMN during target function, the selected biomedical applications such as stimuli-responsive drug delivery, cancer therapy, hyperthermia, wound healing, enzyme immobilization, nucleic acid extraction, tissue engineering, and MRI applications have been attributed to drug encapsulation efficiency, cytotoxicity, folate conjugation and mechanisms, and cell performances.

4.1. Stimuli-responsive drug delivery systems (SRDD)

The new era of nanotechnology brought tremendous impact on cancer therapy from traditional surgery, chemo- and radiotherapy next to immunotherapy. Generally, in terms of its nature and energy, the SRDD system can be categorized as physical, chemical, and biological to deliver drugs to the target cells. Table 4 lists the most commonly used CSMNs in drug delivery systems. CSMN is considered to be a physical form of SRDD system that can be easily controlled via exogenous (EMF) and endogenous (pH) stimuli respectively. For instance, CSMN acts as:

(i) an anticancer drug carrier in the form of methotrexate (MTX) loaded cationic nanocarrier (CTNR) for pH-triggered drug release and in-vitro cellular uptake by MCF7 cell line (Abbasian et al., 2019), curcumin (Cur) loaded CNC@Fe_3O_4 stabilized Pickering emulsion (Cur-MCNC-PE) for EMF-triggered drug release and in-vitro cellular uptake by HCT116 cells (Low et al., 2019), Cur loaded $MnFe_2O_4$–CMC nanocarrier (Cur-MFCMC) for pH-triggered drug release and in-vitro cellular uptake by MCF7 and HeLa cells etc. (Kanagarajan & Thiyagarajan, 2018);
(ii) nano heater in the form of core-shell superparamagnetic nanofluids (CSSNF) for magnetic hyperthermia and in-vitro cellular uptake by brain cancer cells (Leonel et al., 2019) and;
(iii) water-soluble biopolymer ligand to bioconjugate with Doxorubicin (DOX) through amide bonds to form magnetopolymersomes (Fig. 3) for combined effects of chemotherapy and magnetic hyperthermia (MHT) against glioma cells (U87) under EMF (Carvalho et al., 2019).

Since only those molecules needed for cell fitness pass through plasma membranes, only limited success has been achieved in delivering the desired exogenous macromolecules into living cells. The introduction of such molecules into living cells has been permitted through various forms of drug delivery protocols includes: (1) microinjection but only on a single-cell basis (Azarmanesh et al., 2019); (2) electroporation is ideal for bulk delivery applications (Kim et al., 2021), but cell damage is also a common consequence as other forms of cell lysis include sonication, freezing and thawing, osmotic shock, scrape or bead loading, detergent permeabilization, which have been successfully used for specific applications; (3) erythrocyte-mediated cell fusion to deliver large amounts of macromolecules (Magnani & Rossi, 2014) directly into the cytoplasm of cultured cells; (4) receptor-mediated endocytosis systems (Chen et al., 2010) and; (5) liposome-mediated delivery which is used to deliver the conjugation of natural "recognition" ligands to the outer surfaces of the vesicles, allowing some degree of cell-type specificity (Lian & Ho, 2001). Among other delivery protocols, receptor-mediated endocytosis system has been shown natural vitamin endocytosis pathway to deliver desired exogenous macromolecules into living cells through cells internalize vitamins such as folate. Consequently, phenomenal success has been observed in many cases, opening possibilities for useful medical applications.

However, the absence of desired receptors on some cell types, the ultimate deposition of most internalized molecules in the lysosomes, and the low capacities of the uptake pathways have restricted the adoption of this strategy (Lian & Ho, 2001). Furthermore, folate-conjugated exogenous macromolecules could conceivably contact and bind to all cells in a culture medium simultaneously with the lack of cell damage or alterations. It has found that the macromolecule can be nondestructively delivered at reasonable levels into many living cells by the cellular uptake system through folate-receptor endocytosis pathway.

Folate is a natural form of vitamin B9 present in many foods, while folic acid is the synthetic form. The systematically developed CSMN used as Folate-conjugate (FC) by combining folate and it should likewise follow the same course of uptake, namely endocytosis. It is a system of receptor-mediated endocytosis in which the cell absorbs FC through folate-receptor in the same way as natural ligands, such as polypeptide

Table 4
Summary and selected cellulose supported magnetic hybrids for typical drug delivery models, their chemical and physicomagnetic properties.

Cellulose supported magnetic hybrids	Model drug	DLC (%)	DLE (%)	pH	Swelling rate		Drug release			M_S (emu/g)	Magnetism	Reference
					SR wt. (%)	Time (h)	CR (%)	Time (h)	T (°C)			
Chitosan/alginate-Fe_3O_4@CMC with at 2.0 wt. (%) of Fe_3O_4	Dexamethasone	~5.52	~26	1.2	25–27	2 & 5	30–32	10.0	–	–	–	(Karzar Jeddi & Mahkam, 2019)
				5.8	100–120	1 & 3	85–87	10.0	–			
				7.4	65–70	7	25–27	11.0	–			
CMC@$Co_{0.25}Cu_{0.25}Mn_{0.5}Fe_2O_4$	L-3,4-dihydroxyphenylalanine	–	~63	1.2	–	–	~75	~9.5	37	16.00	Ferromagnetic	(Abbasi Pour et al., 2017)
							~84	10.0	40			
				5.8	–	–	~47	~7	37			
							50–55	~10	40			
				7.4	–	–	~55	~7	37			
							58–60	10.0	40			
Fe_3O_4@β-CD/cellulose hydrogel beads with at 0 wt. (%) of Fe_3O_4	5-Fluorouracil	13.26	–	7.4	~25	~3.5	~57	6.5	37	13.40–18.90	Superparamagnetic	(Lin et al., 2019)
Fe_3O_4@β-CD/cellulose hydrogel beads with at 2.0 wt. (%) of Fe_3O_4		11.45	–	7.4	~13	~2.0	~46	12.0	37			
Fe_3O_4@PEP-CMC	Doxorubicin	78.12	74	6.0	–	–	25	6.0	37	–	–	(Elumalai et al., 2015)
Fe_3O_4@CTMB	Racemic ibuprofen	–		–	–	–	~10	–	–	–	–	(Huang et al., 2016)
Fe_3O_4@CNC-tris(2-aminoethyl)amine	Methotrexate	30.40	91	5.4	–	–	~76	150	37	~30	Superparamagnetic	(Rahimi et al., 2017)
							~78	150	40			
				7.4	–	–	~29	150	37			
							~29	150	40			
Fe_3O_4@DAS@DOX@CPEG	Doxorubicin	13.81	42	5.0	–	–	>54	35	–	~40	Superparamagnetic	(Hosseini et al., 2020)
				7.4	–	–	~17	25	–			

DLC = drug loading capacity; DLE = drug loading efficiency; CR = cumulative release; M_s = saturation magnetization; SR = swelling rate; T = temperature; CD = cyclodextrin; PEP = polyelectrolytes protamine; CTMB = cellulose tris-(4-methylbenzoate).

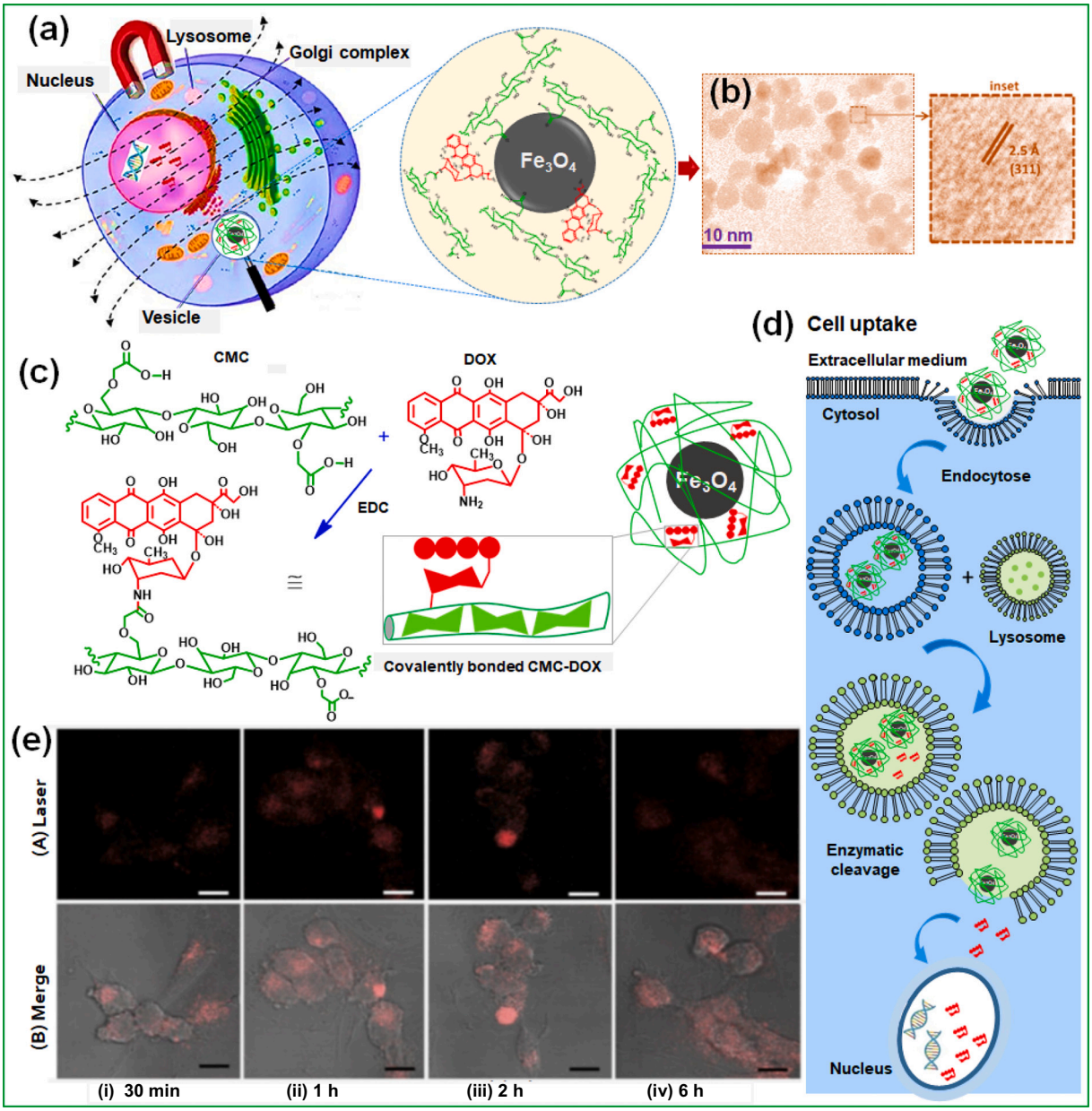

Fig. 3. a) Graphical representation of magnetopolymersomes for potential multimodal brain cancer therapy and the enlargement of the CSMN, b) TEM image of the magnetopolymersomes (inset: HRTEM image with interplanar distance (d = 2.5 Å) between 311 panes of lattice fringes), c) Reaction scheme for covalently bonded CMC-DOX formed between carboxylate groups of CMC and amine groups of DOX through EDC leads to amide covalent bonds, d) Schematic illustration of Fe_3O_4@CMC-DOX internalization and drug delivery process to cells and, e) Confocal laser scanning microscopy images ((A) Photoluminescence image and (B) Photoluminescence image with + bright field images) of cellular uptake of Fe_3O_4@CMC-DOX for U87 cells after incubation for (i) 30 min, (ii) 1 h, (iii) 2 h and (iv) 6 h (scale bar = 10 μm). Adapted and reprinted from Carvalho et al. (2019) with proper permission from Royal Society of Chemistry, (Carvalho et al., 2019).

hormones and viruses are absorbed and they inward budding of the plasma membrane. Therefore, this delivery protocol is used to deliver desired exogenous macromolecules through folate receptor-mediated mechanism into dividing cells, at reasonable rates, and folate is deposited into cytosolic but not lysosomal compartments (Chen et al., 2010). In furtherance, it would seem that many cells are capable of internalizing folate-conjugated macromolecules with sufficient dosage during chemotherapy.

The MHT, on the other hand, is an advanced and promising cancer therapy tool due to; (1) selectively targeting the infected cancer tissues without affecting healthiest tissues; (2) their rapid and sometimes disruptive development and; (3) the lower side-effect compared to traditional chemotherapy and radiotherapy (Cardoso et al., 2018). Owing to its outstanding safety profiles, superparamagnetic behavior, and biocompatibility, Fe_3O_4 NPs offer ample opportunities for advanced materials development to fight against cancer (Ulbrich et al., 2016). In this context, Matos and his colleagues developed Fe_3O_4 NPs integrated cellulose acetate membrane for MHT using the electrospinning technique (Matos et al., 2018). The membrane has demonstrated lower heating ability and almost 100% cell viability for the incorporation of 5 mg/ml Fe_3O_4 NPs. Therefore, the membrane has been classified as a highly successful cancer treatment choice for easily accessible tumors or post-operative treatment with a lower dose of medication and a significant reduction in side effects.

4.1.1. *Multifunctional nanocarriers based SRDD*

The cell proliferation or viability of the nanomaterials is essential and plays a key role in actual biomedical applications as a potential

carrier. In general, the respective pH of 7.4 and 5.0 in the biological blood system and intracellular endosomal/lysosomal acidic conditions inside the cancer cell were used for the cytotoxicity analysis. In this regard, CMC@Fe_3O_4 nanocarriers maintain >100% cell viability of the L929 cell line after 24 h incubation with standard MTT cell assay, while it was observed 92.1% for same concentration 50 mg/ml of naked Fe_3O_4 NPs concentration (Guo et al., 2015). It is clear, CMC's addition to live cells has minimized cytotoxicity. Due to the extracellular and intracellular acidic environments of tumors, the nanocarriers' pH-dependent property facilitate typical benefits to their drug delivery behavior, which can speed up the release of the drug and provide adequate cellular drug uptake or the significant local drug concentration. DOX is a well-known anticancer drug, where 48 h of its cumulative release of 34.3% demonstrate the stability of DOX-loaded CMC@Fe_3O_4 nanocarriers in the physiological environment (pH 7.4), while in an acidic medium (pH 5.0) the release rate was reached 40.7% within 2 h and it continued up to 87.3% for the next 48 h. Because the carboxyl groups in CMC tend to protonate in an acidic condition, which leads to the flagging of interactions between the DOX molecules and the nanocarrier, then DOX becomes more soluble in an acidic condition.

Another study showed that the DAS layer of the nanocarrier (MNP@DAS@DOX) contributes 88% pH sensitive DOX release, while the nanocarrier with CPEG (MNP@DAS@DOX@CPEG) has exhibited only 72% of DOX release at acidic medium (pH 5.0) within 72 h (Hosseini et al., 2020). However, both the DAS and CPEG layers revealed the same DOX release pattern in a neutral medium (pH 7.4) within 30 h, the duration of which was considered to be the lifetime of most of the injected nanocarriers in the blood circulation. Besides, the nanocarriers help selectively targeted applications using an EMF and also enhance the cell cytotoxicity of the cancer tumor.

Recently, MTX loaded CTNR was prepared to increase the anticancer efficacy of MTX in MCF-7 breast cancer cells (Abbasian et al., 2019). The authors developed a triblock terpolymer form of CTNR by in-situ grafting of surface-modified ZnO and Fe_3O_4 NPs, as well as PMADQUAT (cationic monomer) monomers, on xanthate esters functionalized MCC in the presence of an azobisisobutyronitrile free-radical initiator. The functionalization of these NPs was achieved by coating them individually with 3-(Trimethoxysilyl) propyl methacrylate (PAcZnO and PAcFe_3O_4). The selective and effective loading of MTX with a cationic moiety of the CTNR was reported. The electrostatic interactions have emerged to attract the MTX with >98 and 95% of encapsulation efficiency for MCC-g-PMADQUAT-g-PAcZnO and MCC-g-PMADQUAT-g-PAcFe_3O_4, respectively. In vitro cellular cytotoxicity study revealed that the cell viability has dropped to 40% for MTX (100 μg/ml) loaded MCC-g-PMADQUAT-g-PAcFe_3O_4 than free MTX after 48 h exposure with MCF7 cell lines, and it decreased steadily to below 17% when the MTX concentration raised to 200 g/ml. It was also reported that NPs with particle sizes <70 nm were more effective at delivering MTX to cancer tissues on a targeted basis (Abbasian et al., 2019).

Kanagarajan and his colleagues developed Cur-MFCMC nanocarrier as a pH-sensitive drug-releasing agent, which displayed a comparatively higher drug-releasing potential at an endosomal acidic pH 5.5 than that in usual physiological pH 7.4 (Kanagarajan & Thiyagarajan, 2018). The Cur-MFCMC exhibits a higher preferential in vitro cytotoxicity effect on the cancer cells and a reduction in cell viability after incubating MCF7 for 48 h. Also, the MCF7 and HeLa cell lines showed half minimal inhibitory concentration (IC_{50} value) for Cur-MFCMC at 19.36 and 16.20 μg/ml, respectively. The findings indicate that the intracellular Cur concentration of the Cur-MFCMC supplied by $MnFe_2O_4$-CMC-Cur was greater than the free Cur concentration. Hence, the Cur-charged NPs would have greater potential to enter into the cancer cells and show increased pharmacological effect (Kanagarajan & Thiyagarajan, 2018).

4.1.2. Pickering emulsion and colloidal nanoconjugate based SRDD

In recent years, SRDD based on Pickering emulsions (PEs) has proven to be more effective for cancer therapies (Ganguly et al., 2020; Low et al., 2019; Yang & Li, 2018). Because of their colloidal stability, easy encapsulation of different MNPs and other functional macromolecules, and help to protect the drugs from gastrointestinal hydrolysis and enzymatic degradation (Marti-Mestres et al., 2002). In this regard, magneto-responsive PEs have the attractive capability of precisely transporting and disarming the Pickering-based carrier. It is possible due to their emulsifying transportation and ability to demulsify via surface wettability in response to internal or external stimuli such as pH, temperature, ultrasound, and EMF (Low et al., 2019). As a result, (1) the strong solid film barrier that forms around the emulsion droplet surfaces can be turned off. The formation of such a film is caused by the irreversible adsorption of colloidal solid (micro−/nano-) particles at the interfaces of two immiscible liquids and; (2) the ability to unlock the restriction of PEs to be used in biomedical applications is allowed by temporal stability and subsequent remotely implied destabilization, that could possibly occur by disordering the superior shielding effects imparted by solid particles. For instance, the net negative surface charge −62.19 mV of CNC has significantly lowered to −25.37 mV after the in-situ co-precipitation of Fe_3O_4 NPs by reducing its surface hydrophilic groups (-OH groups). Thus, the hydrophobicity of CNC@Fe_3O_4 based PE-based smart carriers (PESC) has been increased, resulting in improved emulsifying transportation. It further improved the efficacy of the PE stabilized magnetic biopolymer through the magnetic as well as pH responsiveness (Low et al., 2019). However, the stability of the PESC interrupted at $7.5 \leq pH \geq 8.5$ in the presence of oscillating EMF, while it can remain be physically stable at $1.5 \leq pH \geq 6.5$.

In contrast, MHT ablation of tumors through an injectable Pickering-based nanocarrier containing Fe_3O_4, hydroxypropyl methylcellulose (HPMC), and polyvinyl alcohol (PVA) (Fe_3O_4@HPMC/PVA) was investigated (Wang et al., 2017). As prepared CSMN showed high efficiency for the cancer tumors, in which 0.06 ml of Fe_3O_4@HPMC/PVA (6:3:1) ablated the tumors completely after 180 s of induction heating through minimally invasive magnetic ablation. Fig. 4(a–f) illustrate this tumor ablation progress using injectable and thermally contractible nanocarrier.

The efficiency of colloidal nanoconjugate-based SRDD systems is influenced by the doping of Fe_3O_4 with other transition metals and the properties of the encapsulating polymer matrix. For instance, Cobalt-doping provides a significant enhancement in the magnetic anisotropy of the system by a partial replacement of Fe^{2+} by Co^{2+} species, resulting in a decrease in the ion radius and a shrinkage of the Fe_3O_4 nanocrystal unit cell, which subsequently increases the magnetic anisotropy of the system, that improve MHT (Fantechi et al., 2015).

However, the amalgamation of Co^{2+} in Fe_3O_4 sometime can disable the effect on the anisotropy of the system by their expanded hydrodynamic volume ($\uparrow d_h$) and, introduce lower heating rate compared to free Fe_3O_4 NPs (Das et al., 2021). In contrast, CMC encapsulation contributes for the reduction in MHT responses, which caused by forming larger $\uparrow d_h$ using their negative charges (—COO—) through: (1) neutralization process based on water molecules at the outer surface of the nanoconjugate and; (2) interaction with Co^{2+} present at the surface of the Fe_3O_4 NPs. As a result, d_h overcoming the effect on the anisotropy of the system, that relative to a decrease of the mass of MNPs per volume of nanoconjugate. Therefore, the MHT effect of the nanoconjugates has been solely dependent on the Fe_3O_4 NPs, with higher Fe_3O_4 NPs exhibiting a faster heating rate.

The cytotoxicity study of the CMC@Fe_3O_4 colloidal nanoconjugate exhibits over 80% of cell viability responses, in which MTT bioassay has been incubated together with cancer (U87) cells and CMC@Fe_3O_4 nanoconjugate. However, cell viability responses dropped to <70% (recommended level) when the nanoconjugate concentration increased, representing the nanoconjugate's cytotoxicity effect (Leonel et al., 2019). Because Fe_3O_4 interferes with and disrupts cellular metabolism at higher concentrations. However, the negative charge (—COO—) of the CMC surface does not affect the cytotoxicity response at higher concentrations, while it can cause an alteration of the electrostatic

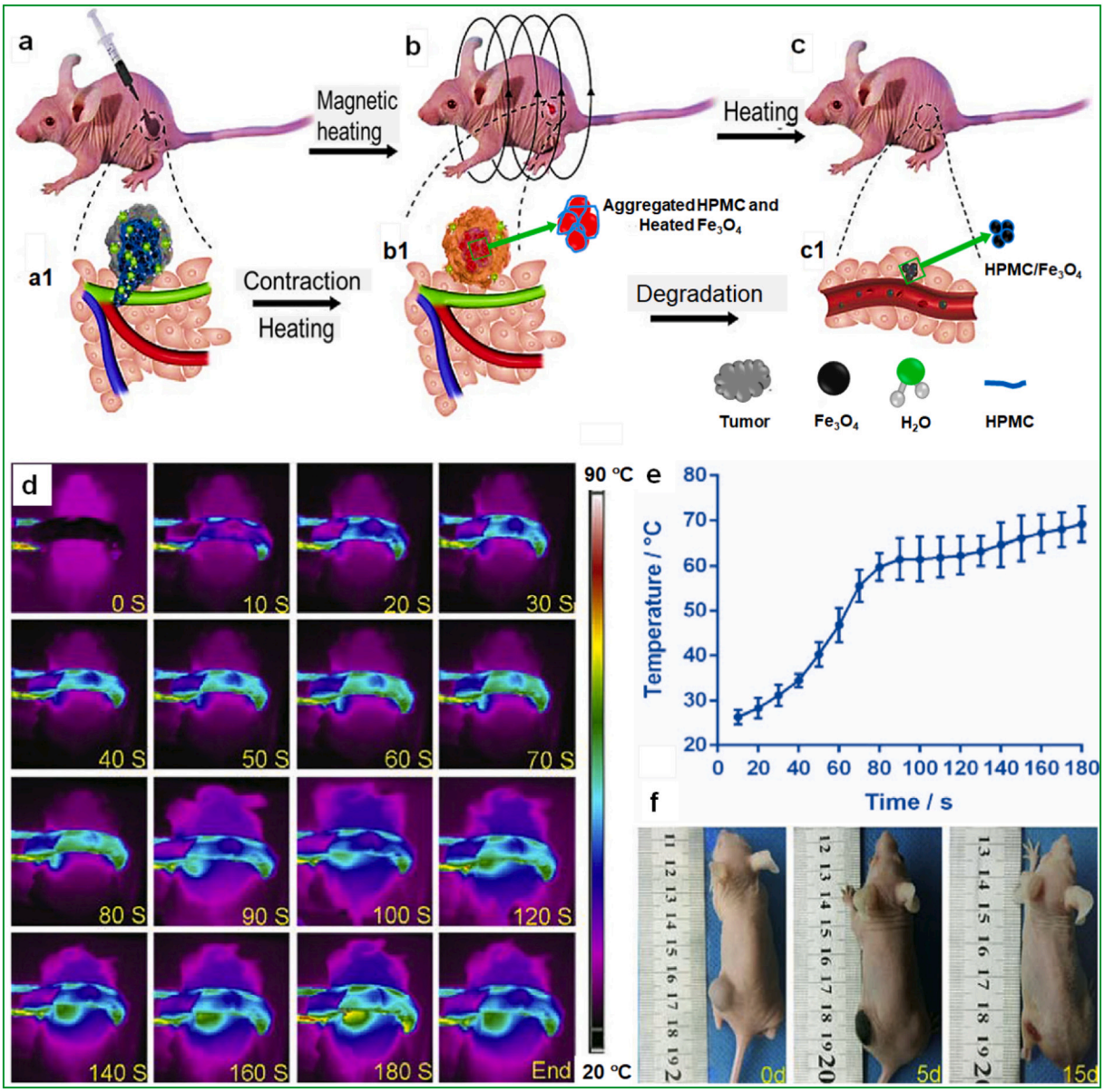

Fig. 4. Injectable and thermally contractible HPMC/Fe_3O_4. a) The injection of the HPMC/Fe_3O_4 material into the tumor. a1) The formation of "tail"-like leakage of the HPMC/Fe_3O_4 material inside the tumor and their closeness to the adjacent important normal structures (green, red and blue vessels). b) AMF: HPMC/Fe_3O_4 contracts after heating (red color represents the increased temperature of HPMC/Fe_3O_4). b1) Heated HPMC/Fe_3O_4 inside the tumor and the disappearance of its "tail". c) Vanishing of a tumor. c1) HPMC/Fe_3O_4 degradation. Magnetic hyperthermia ablation efficiency in vivo: d) Thermal images of tumors containing 0.06 ml of HPMC/Fe_3O_4 after magnetic heating for 180 s. e) Temperature-time curve. f) Macroscopic changes in tumors at the time points of 5 days and 15 days after magnetic hyperthermia ablation treatment Adapted and reprinted from F. Wang et al. (2017) with proper permission from Elsevier, (F. Wang et al., 2017).

interactions at the cell-nanoconjugates interfaces. In furtherance, due to lack of selectivity and specificity for killing cancer cells, it is necessary to make biofunctionalization of CMC with specific molecules (folic acid, peptides, antibodies, etc.) before submitting target cancer cells to MT assay.

4.1.3. *Folate-conjugates based SRDD*

The efficacy of the folate conjugate (FC)-mediated drug delivery protocol is often overestimated in many cancers such as breast, brain cervical, colorectal, renal, nasopharyngeal, ovarian, and endometrial, as well as a large number of tumors such as carcinoma and brain tumors by combining folate with nanomaterials (Sunderland et al., 2006). The CMC surface has been used as a folate implantable basement in a variety of multi-functional nanovector (NV) synthesis studies, resulting in CSMNs serving as the target FC. It was found that the FC based nanocarrier exhibited high intracellular drug release efficiency (Kang et al., 2015). The presence of FC in multiple pH-responsive chemotherapeutic agent nanocarriers enables the nanocarrier to act as dual sensitive tumor targeting (Chen et al., 2017; Pourjavadi et al., 2016). The chemistry behind this FC mechanism related to the CMC surface is illustrated in Scheme 2. This conjugation mechanism has been aided by the N-(3-dimethyl aminopropyl)-N′-ethyl carbodiimidehydrochloride (EDC) and the N-hydroxysuccinimide (NHS), in which:

(i) EDC is used to activate the carboxyl groups present in folic acid and CMC′ surface that generates an active intermediate product acyl-isourea and;
(ii) the addition of NHS initiates the nucleophilic attack on carbonyl carbon of acyl-isourea, resulting in the formation of a reaction intermediate. The reaction continues with the nucleophilic attack

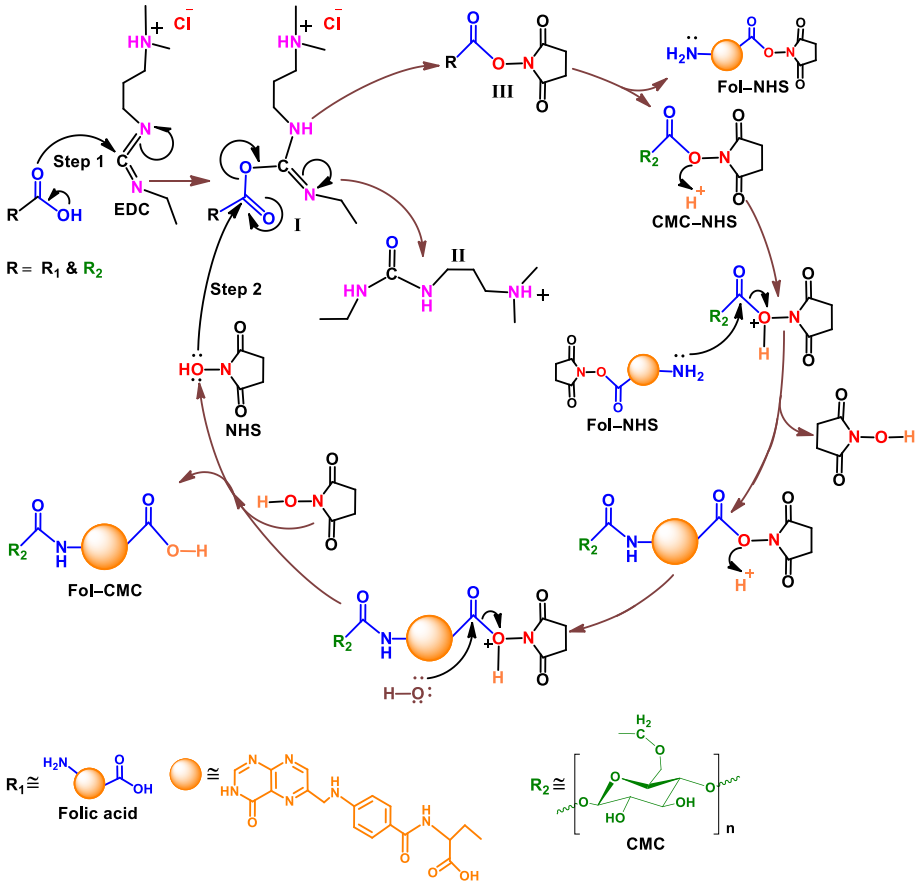

Scheme 2. The proposed reaction mechanism for EDC-NHS chemistry in the carboxylic acid system has been adapted in line with previous studies (Bart et al., 2009; Bergfeld et al., 2012; Jaetao et al., 2009; Kazenwadel et al., 2015; Mahalunkar et al., 2019; Olsson et al., 2012). EDC reacts with the carboxylic acid groups on the surface of the folic acid and CMC to forms an amine-reactive O-acylisoure intermediate (I). The nucleophilic attack of NHS' oxygen ion on this intermediate initiate a variety of electron rearrangement mechanisms. As the result, both substrates yield an isourea byproduct (II) and semi-stable amine-reactive NHS-esters (III) (a mixture of CMC-NHS and Fol-NHS).

of the primary amine groups of the Fol-NHS on protonated CMC-NHS. As a result, the CMC-NHS stabilizes the semi-stable amine-reactive NHS-ester by converting it into Fol-CMC as the final product. It is a continuous process that will continue until EDC is completed.

Interestingly, Sivakumar and Co-workers reported FC-CMC@MNP/5-FU based magnetic NV as a theragnostic system (Fig. 5) (Sivakumar et al., 2013). The NV was created through a stepwise synthesis in which folate was first attached to the CMC via an EDS-NHS coupled reaction, as shown in Scheme 2, resulting in the formation of a —CO—NH bond. Therefore, negatively charged (—COO^-) Fol-CMC's surface provide amble opportunity for; (1) an anticancer drug (2,4-Dihydroxy-5-fluorouracil (5-FU)) loading into Fol-CMC, in which 1% of $CaCl_2$ has been used for ionic cross-linking between Fol-CMC macromolecules through chelation mechanism. As a result, the theragnostic system demonstrated 89% of 5-FU encapsulation efficiency; (2) Fe_3O_4 NPs loading by nucleation mechanism on their surface to generate CSMN (Yee et al., 2019), in which the Fe_3O_4 NPs were attracted to the negatively charged (—COO^-) Fol-CMC's surface and; (3) labeling of imaging moiety (Fluorescein-5-isothiocyanate (FITC)) through amidation mechanism to synthesis NV (Sivakumar et al., 2013).

FITC is a fluorescence dye and belongs to the xanthene dyes generally used for labeling different biomolecules. The nucleophilic attack of Fol-CMC's carbonyl oxygen on the carbon atom of the FITC's isothiocyanate (—N═C═S) group is triggering amide formation in phosphate buffer solution at pH 7.4. The study reported better fluorescence signals and efficient internalizations through cellular imaging of the NV after being treated with a human breast cancer cell line (MCF7 cells) and a glial cell line (G1 cells) (Fig. 5(a–i)).

Cell cytotoxicity analysis revealed that the cell viability of both MCF7 and G1 cells: (1) decreased as a function of their incubation period with NV to 59 and 55% after 24 h in the presence of Alamar blue assay at 4 mg/ml of NV, which was continuously fallen up to 34 and 32% when the incubation period extends to 48 h; (2) decreased to 34 and 32% after immediate MHT treatment and continued to decline further to 25 and 23% when the concentrations of NV increased from 2 to 4 mg/ml, respectively and; (3) decreased to 19 and 15%, and continued to decline up to 6 and 4% concerning MHT treatment after 12 and 24 h of the incubation period for 4 mg/ml of NV. It has been noticed that almost 95% of the cancer cells had been synergistically killed via combined treatments of the NV and MHT, compared to 5-FU-free NV. The observations revealed that the incubation period and the concentration of the NV played an important role in the cell viability and cytotoxicity of the cancer cell.

4.1.4. *Hydrogel beads based SRDD*

Stimuli-responsive hydrogel beads based on CSMN are popular in pharmaceutical application owing to their high release performance, large potential in drug loading capacity, and good biocompatibility (Karzar Jeddi & Mahkam, 2019). To control the dosage and drug-releasing rate, the efficiency of CSMN hydrogel beads can be adjusted by tuning the EMF, pH and the amount of MNPs.

The EMF and pH-based stimuli can help to deform the beads' 3D network by extending and weakening their bonds due to the degree of swelling. Once the beads network reached a high degree of swelling, the pore size becomes larger, hence the drug can easily diffuse into the solution (Bardajee et al., 2014). Therefore, CSMN beads become more attractive for disease treatment like diabetes requiring variable dosage and drug delivery timing (Lin et al., 2019). This attribute is because its drug release behavior can be easily tuned by an EMF through noncontact external stimuli. Interestingly, Lin and Co-workers developed remotely

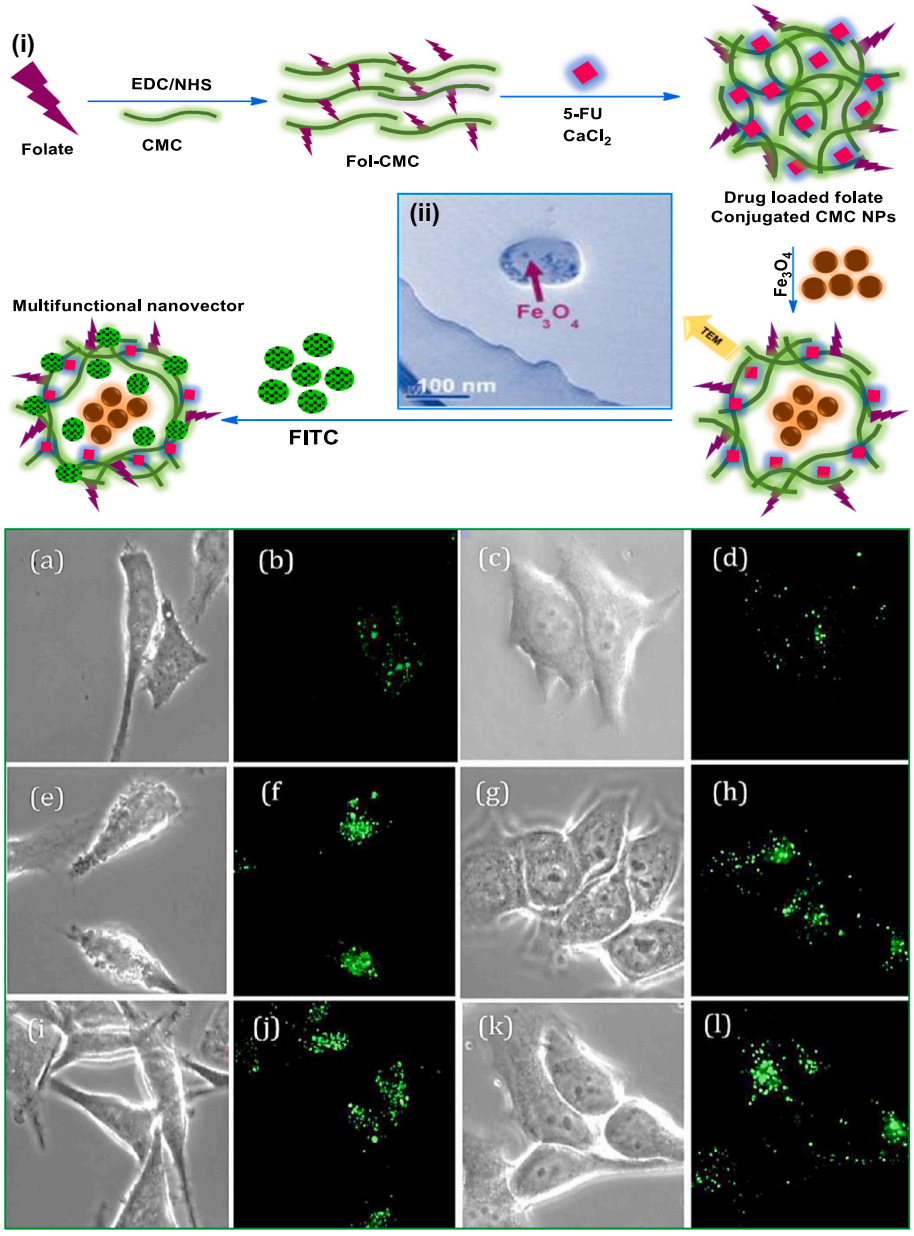

Fig. 5. (i) Schematic of the stepwise synthesis of multi-functional nanovector and (ii) TEM image of CMC encapsulated Fe_3O_4 NPs (average size of 100–150 nm). Bright-field images of (a, e, i) G1 and (c, g, k) MCF7 at 1, 2, and 4 h and confocal fluorescence of (b, f, j) G1 and (d, h, l) MCF7 treated with NPs for 1, 2, and 4 h. Adapted and reprinted from Sivakumar et al. (2013) with proper permission from American Chemical Society (Sivakumar et al., 2013).

controlled drug-releasing beads based on Cellulose@Fe_3O_4/β-CD-hydrogel to study their performance (Lin et al., 2019). The beads exhibit better drug loading capacity, cytocompatibility, and stepwise controlled drug release of the 5-FU model drug. The drug release rate was controlled by the content of Fe_3O_4 NPs through EMF, where the beads released the drug at 37 °C when the EMF was turned off. As an advantage, the beads capped the drug up to 720 min by controlled drug release for their extended continuous stepwise release, while the beads without MNPs displayed passive drug release up to 360 min. The beads get deformed 3D network structure and lost drug release capability due to the alignment and attraction of the Fe_3O_4 incorporate cellulose when EMF turned on caused pore size decrease that led to the drug being blocked within the beads.

By contrast, Karzar and colleagues reported pH-sensitive alginate-CMC@Fe_3O_4/chitosan beads with high drug loading and releasing potential as well as excellent swelling properties (Karzar Jeddi & Mahkam, 2019). The second chitosan layer has been used to retain the beads' shape from deforming. The beads only released 29.5 and 26.9% of the dexamethasone model drug at pH 1.2 and pH 7.4 respectively. Because the beads became more stable and dexamethasone showed low solubility at acidic medium, while strong hydrogen bonds and weakly soluble nature of the chitosan in a basic medium, indicate the reason why drug release drops. However, it was found that within 10 h, the beads had released 90% of the drug at pH 5.8. Subramaniam and his colleagues prepared CNC supported magnetic alginate beads to study their pH sensitivity for drug delivery application (Supramaniam et al., 2018). They used Ibuprofen as a model drug, in which almost 100% drug was released within 330 min. However, the efficiency of drug encapsulation depends on the form of cellulose support used in building the beads, and the amount of drugs used in the sample (Supramaniam et al., 2018). Therefore, this type of novel CSMN beads can be systematically designed for control drug delivery carriers that integrate $CoFe_2O_4$ and $MnFe_2O_4$ NPs with other form of celluloses such as hydroxyethyl cellulose, BC and so on. As a result, significant physicomagnetic properties, aspect ratios,

and porous structures can be achieved, leading to improved drug encapsulation efficiency and drug release mechanisms.

4.2. Wound healing

CSMN has been used as a potential smart material for wound healing applications. Wound healing is a physiological response that is like other responses such as, embryonic development, and pathological processes (i.e., tumorigenesis and atherosclerosis) that may alter tissue stiffness (Pramanik et al., 2019). Particularly, in the current development of wound dressing, the MNPs are being grafted onto the cellulose fibers as a key process of smart bandage to monitor the wound healing capacity of the bandage. The main aim of this use of the MNP in wound dressing is to make it sensitive as a wound healing biomarker. For example, it is used to determine the proper temperature, to detect and respond to temperature changes owing to the cellular activities at a wound site. In the recent report, authors have used $CoFe_2O_4$ NPs to magnetize the cellulose (Williams et al., 2019). They grafted these MNPs onto cellulose fibers owing to their unique structural, physical, and magnetic properties. The wound dressing was first functionalized with branched polyethyleneimine (PEI) to attach the NPs onto the cellulose fibers. In this essential step, the β-PEI can able to bind to cellulose fibers successfully and it contains multiple amino groups capable of chelating metal ions as reported by other researchers (Wågberg, 2000).

Besides, poly(ether ether ketone), (PEEK) or poly(oxy-1,4-phenyleneoxy-1,4-phenylenecarbonyl-1,4-phenylene), with carboxylic functionalization can also be used to replace the β-PEI to provide maximum binding sites to the cellulose (Pramanik & Kar, 2012). However, to remove all unbound entities, grafted with $CoFe_2O_4$, from the wound dressing NPs complex, the polyethylene glycol (2 ppm) can be used to wash after the wound dressing. A schematic illustration of the design of the smart wound dressing is shown in Fig. S3. It depicts the MNPs grafted and aligned scaffolds, which are placed on the cellulose inner gauze of the wound dressing.

4.3. Enzyme immobilization

The immobilization of the native enzyme is necessary due to its narrow pH range, high thermal sensitivity and difficulty in recovery and reuse. Besides, the enzyme activity could be decreased by conformational changes that occurred in their molecular structure. These changes can happen through their frequent treatments including, thermal exposure, washing with buffer, and reusing in a new reaction cycle (Xue et al., 2019). In furtherance, due to poor operation stability, difficulties in recovery, reuse, and the high cost of free enzymes make them limited for further applications. Therefore, a successful enzyme immobilization technique associated with other functional materials can overcomes these issues and improves their properties, such as stability, easy recovery and simple reusability. In this regard, the use of CSMN in the field of proteins/enzymes immobilization is regularly associated with different biomedical applications, such as in the treatment of various diseases and diagnosis. In general, the ideal immobilization technique should satisfy main three requirements as follows: (1) the high specific surface area, easily recyclable, excellent biocompatibility, and large binding capabilities to the enzyme with the recovery of enzymatic activity should be exhibited by enzyme carriers; (2) the simple, mild and rapid immobilization process should be there and; (3) the good stability should be exhibited by the immobilized enzyme (Cao et al., 2015).

In this context, chemical immobilization can prevent enzyme denaturation (Peng et al., 2019) better than physical adsorption (Guo et al., 2018) and encapsulation-based enzyme immobilization (Drout et al., 2019; Li, Li, et al., 2020; Tamaddon et al., 2020). It forms a covalent link between the enzyme and the support to improve the conformational stability of the immobilized enzyme. As a result, glutaraldehyde (GA) has been used for chemical immobilization in many studies of MNPs-associated enzymes such as tyrosinase, lipase, α-amylase, and acetyl xylan esterase immobilizations (Cao et al., 2015). However, GA-based crosslinks can change the ionization due to the basic or acidic amino acid side chain of the enzymes in the microenvironment, which surrounds the catalytic site of the enzyme or the surface group of the CSMN.

Usually, core-shell structured CSMN has outstanding chemical stability and high magnetic reactivity, most notably low bio-toxicity and low-cost synthesis, making them a promising candidate to expand the scope of application of enzyme immobilization. Recently, the CSMN based on BTCA functionalized MCC has been reported to study their operational stability and the activity of the immobilized enzyme molecules (Xue et al., 2019). They found that lysozyme immobilized CSMN retains its enzymatic activity at higher temperatures better than native lysozyme by showing 73.9% relative activity at 60 °C, where native enzyme exhibits only 49.9%. Also, the immobilized enzyme structure's conformational integrity and its storage stability revealed its multipoint covalent fixation, which ultimately prevents enzyme dissociation from the carrier and enzyme inactivation into storage.

Besides, core-shell structured CSMNs with promising cellulose surface functionality are being preferred for use in an effective enzyme immobilization via chemical immobilization. Consequently, the cellulose acts as a shell layer of the magnetic core via covalent linkage. In this regard, epoxy-active support is nearly ideal for developing a successful immobilization route for the enzyme (Lei et al., 2009; Luo & Zhang, 2010). Because the epoxy groups on the CSMN surface form covalent bonds with enzymes through their ring-opening reaction. It was also found that the epoxy groups are extremely stable at neutral pH, even in wet environments. Fig. 6(a). shows the epoxy-based surface activation of the core-shell structure CSMN and its enzyme immobilization. Moreover, epoxy supports can react with different nucleophilic functional groups (e.g., amino, hydroxyl, or thiol moieties) of the protein (Scheme 3) (Lei et al., 2009).

However, other surface modifications such as carboxyl groups, (Bullard et al., 2020; Heise et al., 2020; Liu et al., 2017; Tao et al., 2020) and amino functionalization (Alatawi et al., 2018; Xin et al., 2018) of this type of CSMN's —OH groups have also been reported for an excellent covalent enzyme immobilization (Sharifi et al., 2019; Zhang et al., 2020).

Tamaddon and colleagues used dialdehyde modified MCC@γ-Fe_2O_3 and CNC@γ-Fe_2O_3 based CSMNs to immobilize urease, in which CNC@γ-Fe_2O_3/urease exhibited higher residual activity than MCC@γ-Fe_2O_3/urease (Tamaddon et al., 2020). However, the sensitivity of the urease immobilized CSMNs against pH and temperature changes became poor due to strong covalent bonds formed between urease and prepared CSMNs.

In contrast, magnetic CNC has successfully been used for GOx (Yee et al., 2019), peroxidase (Zengin Kurt et al., 2017), lysozyme (Xue et al., 2019), and papain (J. Xiong et al., 2020) enzyme immobilization with enhanced stability, activity, and catalytic efficiency. Yee and Co-workers performed GOx immobilization using CNC-COOH@Fe_3O_4 (CNC-COOH@Fe_3O_4/GOx) through carbodiimide-coupling reaction, where electrostatic self-assembly technique has been used to integrate the MNPs into CNC-COOH (Yee et al., 2019). The CNC-COOH@Fe_3O_4/GOx was utilized to detect glucose molecules, and it demonstrated a higher affinity for glucose molecules compared to free GOx, as well as long-term storage stability, complete recovery and reusability after 10 consecutive cycles. Table 5 listed some typical enzymes with their loading period, capacity and recovery, and properties of stability, as well as reusability after the 5th cycles of CSMN.

4.4. Nucleic acid extraction

Over the decades, a variety of nucleic acid extraction techniques have been documented, some of which are listed to assist readers: (1) conventional extraction techniques such as, guanidinium thiocyanate-phenol-chloroform extraction (Dimke et al., 2021; Zavala-Alvarado & Benaroudj, 2020), alkaline extraction method (Wang, Zhao, et al., 2020;

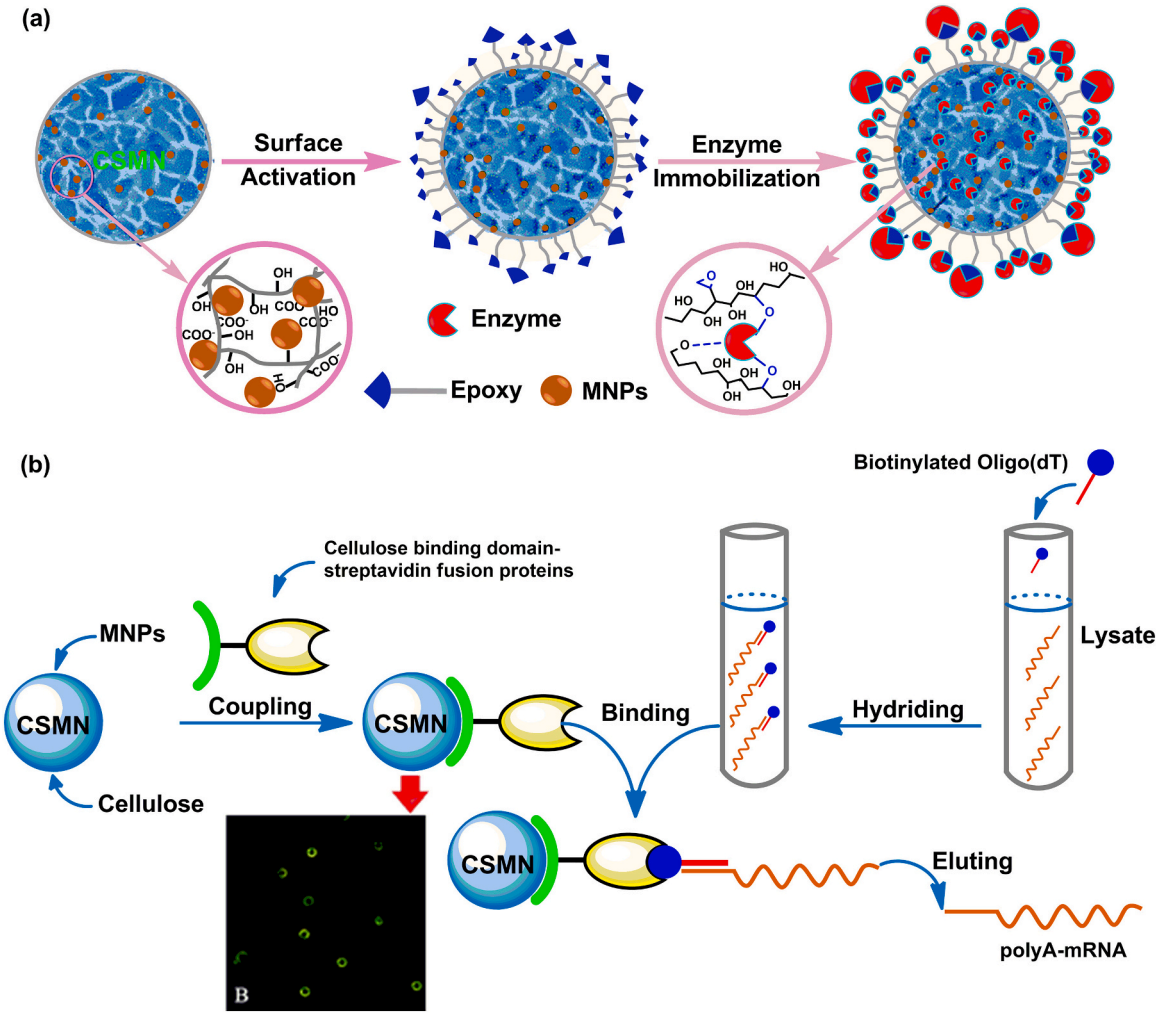

Fig. 6. Graphical representation of: (a) the activation of epoxy and immobilization of enzyme in the CSMN. Adapted and reprinted from Gao et al. (2009) with proper permission from Elsevier, (Gao et al., 2009) and; (b) the mRNA isolation steps of Streptavidin fusion protein using CSMN. Insert (B), laser scanning confocal microscopic image confirms the binding identification of cellulose-binding domain-enhanced green fluorescent protein to CSMN at the excitation wavelength of 488 nm. Adapted and reprinted from Gao et al. (2009) with proper permission from Elsevier, (Gao et al., 2009).

Wang, Zhu, et al., 2020), cetyltrimethylammonium bromide extraction method (Ryan et al., 2020; Verma & Biswas, 2020), ethidium bromide (EtBr)/cesium chloride gradient centrifugation (Liu, Berrido, et al., 2017; Thapar & Demple, 2019), oligo(dT)-cellulose chromatography (Engel et al., 2020; Green & Sambrook, 2018); (2) all-in-one biomolecules extraction (Shahwan et al., 2020); (3) automated extraction system (Dimke et al., 2021; Zhao et al., 2020) and; (4) solid-phase nucleic acid extraction (SPNAE).

The SPNAE is a rapid purification technique compared to conventional methods. The SPNAE includes silica matrices (Asencio et al., 2018; Esser et al., 2006), the mixture of silica gel and glass particles which are used in the presence of chaotropic salts solution (Tan & Yiap, 2009), diatomaceous earth (Liu et al., 2018; F. Zhao et al., 2018), anion-exchange materials (Emaus et al., 2020; Zhu et al., 2020), and magnetic materials such as, metal-organic framework (Meng et al., 2020; Sun et al., 2020), beads (Gao et al., 2009; Li et al., 2018; Wang, Zhao, et al., 2020; Yamazaki et al., 2020), and so on. In general, SPNAE entails four key steps: cell lysis/alkaline lysis, nucleic acid adsorption, cleaning, and elution. However, the cell lysis technique is time-consuming and cannot be used to extract temperature-sensitive cellular components. Based on protocol, alkaline lysis is modified and consequently, it formed a binding between the nucleic acid and the magnetic particles. The beads-based magnetic materials are used in nucleic acid adsorption which does involve with any organic solvents and thus, they eliminate the need for repeated centrifugation, column separation or vacuum filtration. Therefore, magnetic tool is employed to detect the magnetic particles along with the bound nucleic acid. The contaminants are removed by washing with a suitable buffered solution. Then, the nucleic acid is separated from the MNPs with a suitable elution buffer (Tan & Yiap, 2009).

Interestingly, messenger RNA (mRNA) harvesting from eukaryotic cells and tissues with magnetic microsphere was performed via SPNAE (Gao et al., 2009). Initially, ferrofluids and purified cotton were used for the microsphere synthesis to isolate mRNA from different sources. In a typical mRNA eluting mechanism, microspheres are coated with streptavidin fusion proteins through their cellulose binding domain (Fig. 6 (b)), which then act as a scavenger to bind biotinylated oligo(dT) hybridized eukaryotic mRNA. Most eukaryotic mRNAs have tracts of poly (A) tails that hybridize with oligo(dT) matrix and serve as a protein translation template (Sarkar & Irudayaraj, 2008). It helps to make 1 to 2% of mRNA extraction from total RNA. Then, it is separated from oligo (dT)-cellulose via affinity chromatography process. The microspheres are then allowed to settle down at the bottom of a tube and then, it directly removes mRNA from total RNA. In addition, the microspheres maintain the purity of mRNA by reducing the nonspecific binding of many other nucleic acids.

In advance, Li and Co-workers used a CMC@Fe_3O_4 based microsphere to extract and analyze indole-3-acetic acid from plant tissues (Li

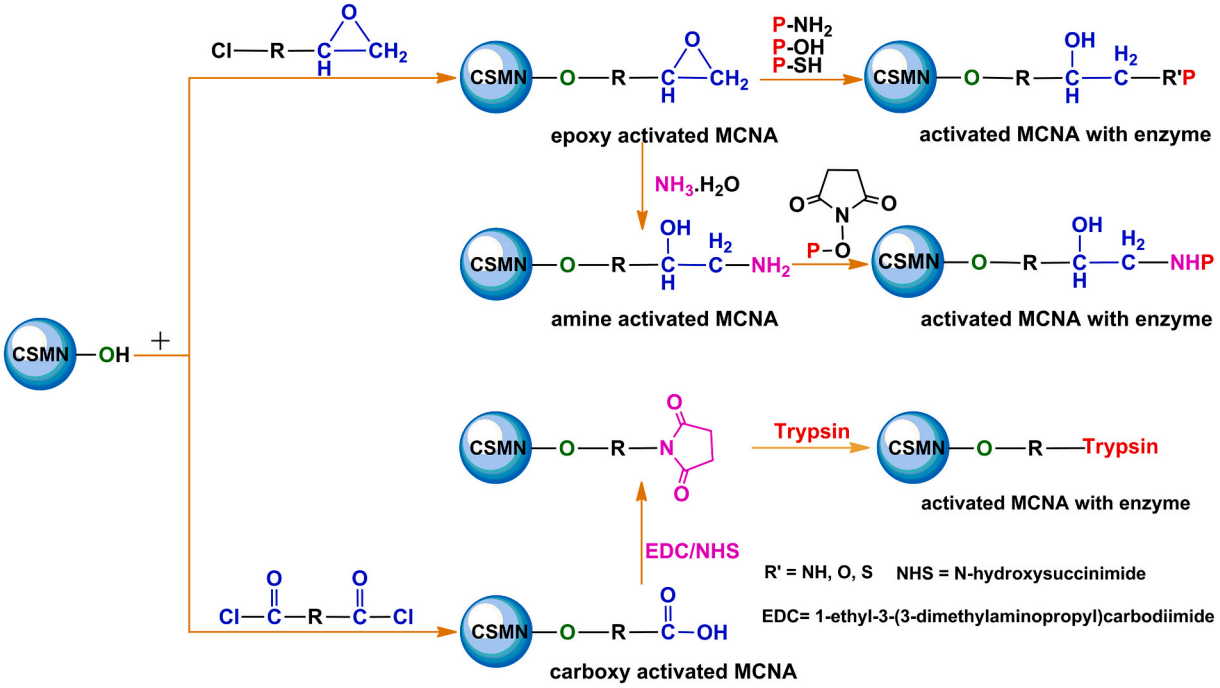

Scheme 3. The reaction scheme of the selected surface modifications of CSMN and their enzyme immobilization.

et al., 2018), where silylated β-CD, indole-3-acetic acid (IAA), and 4-vinylpyridine have been incorporated as template and monomer respectively to select the specific recognition cavities. The result shows that as-prepared microspheres with the size 50–180 μm are appropriate for the detection of the IAA at trace levels in complicated samples, with stable and reliable extraction and can be used multiple times. Generally, SPNAE demonstrates an excellent repertoire of benefits by utilizing a biospecific connection via specific binding between a protein and the CSMN. This includes efficient and comfortable preparation, the removal of toxic compounds, and the use of highly efficient antibodies. The resulting extraction of a pure target molecule by this technique is both convenient and efficient.

4.5. Tissue engineering application

In recent years, biopolymers are emerging at the forefront of vascular tissue regeneration. The skin cells are made up of composites based on collagen, including different proteins and lipids. In tissue-engineered vascular graft (TEVG) technology, biologically active cells are used to achieve regrowth and remodeling of injured tissues, but due to high hemodynamic shear stress at the damaged site, the process gets delayed. Moreover, synthetic vascular grafts cannot be used in small vessels because of graft failure caused by thrombosis and neointima formation. Consequently, to overcome this limitation, Pislaru and colleagues implemented rapid endothelialization using magnetic graft techniques in 2006 (Pislaru et al., 2006). A positive response was seen to improve re-endothelialization when endothelial cells were captured and retained with paramagnetic particles especially in arteries of small diameter (Fig. 7(a & a1)).

Arias and his colleagues developed BC-based magnetic pellicles (BC@Fe_3O_4) and their hydrogel, where BC@Fe_3O_4 was coated with dextran to protect the embedded Fe_3O_4 NPs against oxidation (Arias et al., 2018). The authors used Langevin's function, which predicts that the magnetization of a superparamagnetic material is directly proportional to the concentration of MNPs at ambient temperature with alternating EMF, even if MNPs are rigidly fixed to the material. The proton exchange reactions caused by metallic iron present in the reaction vessel are believed to build bridges between adjacent fibers through cellulose's —OH groups. Therefore, human aortic smooth muscle cells (HASMCs) used to investigate the adhesion properties of the hydrogel by continuous 0.3 T magnetic acceleration using a parallel-plate flow chamber. Interestingly, they found dextran-coated BC@Fe_3O_4 significantly reduces cell adhesion by twofold even at a lower concentration of 25 mM of Fe_3O_4, due to offering lower cell coverage, while higher cell density retention observed when it incubated with collagen. In furtherance, as prepared hydrogel accelerates re-endothelization by facilitating high-cell density coverage of the vascular defect.

Besides, the superparamagnetism and mechanical properties (Young Modulus between 200 and 380 kPa) of this hydrogel suggested that it would be better suited for use in vascular graft applications. An in vitro study showed (Fig. 7(j & k)) that the BC@Fe_3O_4 captured the HAMSCs under the pulsatile fluid flow conditions at the concentrations of 50 mM and 100 mM of iron salt (Arias et al., 2018).

Recently, a scaffold based on nano-HA coated BC@Fe_3O_4 membrane has been reported for bone tissue engineering (Torgbo & Sukyai, 2019). The scaffold had some unique features, such as: (1) increased porosity (around 80%) led to a loss in crystallinity; (2) loss in crystallinity from 82.5% to 62% due to the glucopyranose rings opening, which then led to destroy the ordered packing in the BC and thus gets into the scaffolds easily; (3) surface area rises, which have affected on thermal stability and; (4) the decrease in M_s due to loss in crystallinity structure and oscillation effect caused by the ultrasonication used to disperse the HA and Fe_3O_4. The higher porosity along with interconnected micro-pores promotes uniform cell distribution, cell ingrowth, and neo-vascularization through the scaffold in bone regeneration applications (Torgbo & Sukyai, 2019).

4.6. Magnetic resonance imaging (MRI)

The MRI is a noninvasive and nonradioactive technique, has widely been used in the clinical diagnosis of various tumors with an excellent spatial resolution (Zhang, Liu, et al., 2018). Since conventional MR images have low resolution, MRI contrast agents are used to improve image quality (Hosseini et al., 2020). The contrast agents can be categorized based on magnetic properties depending upon the existence of the magnetic particles such as paramagnetic including, Gd-chelates,

Table 5
Summary and selected cellulose supported magnetic nanohybrids for enzyme immobilization, enzymes and their enzymatic properties.

Cellulose Supported Magnetic Nanohybrids	Enzyme				Stability								RU	Reference
	Type	Loading period (h)	Loading capacity (mg/g)	Recovery (%)	pH	Time (h)	Initial activity (%)	Enzyme activity				Residual activity (%)	After 5th cycles (%)	
								Solvent	pH	T (°C)	ICT (h)			
Magnetic CNC (MCNC)	Papain	2	333	80	7.0–9.0 & 5.0–6.0	1	>83	NBA CU-DES [Bmim]I [Amim]BF_4	5–9	30	2	~94 ~93 ~83 ~78	88	(Cao et al., 2015)
Magnetic cellulose nanocrystals	Glucose oxidase	1	~20[a]	33	5.0	7 × 24	100	SAB	5	RT	–	70	100	(Yee et al., 2019)
Cationic Polyethyleneimine modified Fe_3O_4@CNCs	Papain	1	9	–	7	15 × 24	~92	Phosphate buffer	– ~7	40 –	1	~23 100	~98	(F. Zhang et al., 2016)
CMC-based core-shell structured magnetic cellulose microsphere (CSMNS)	Prenyltransferase NovQ	4	–	–	8.5	40 × 24	65	Tris−HCl, menadione hydroquinol, DMAPP & $MgCl_2$	8.5	35	5	67	~89	(W. Ni et al., 2020)
Cellulose-based CSMNS	Lysozyme	8–24	~80	~79	6.0–7.0	40 × 24	~69	Phosphate buffer	7	40	1	98	60	(Xue et al., 2019)
Acidic-nanocellulose@Fe_3O_4	Fungal β-galactosidases[AO]	2	~98	94	6.2–6.7	48	~89	Buffer sodium acetate	4.5	68[SF]	3	–	–	(A. Gennari et al., 2019)
	Fungal β-galactosidases[KI]	24	~82	79	–		–		7.0	60[SF]	24	–		
Basic-nanocellulose@Fe_3O_4	Fungal β-galactosidases[KI]	3	~87											
	Fungal β-galactosidases[AO]	24	~81	94	6.2–6.7		~89		4.5	68[SF]	3	–		
Fe_3O_4–cellulose nanospheres	Lipase[G]	15	560	–	7.5	6	–	Tris-HCl, & p-NPP	4.8	55	15	–	100	(Bandikari et al., 2018)
Nano-cellulose@Fe_3O_4	Halo-tolerant glutaminase[B]	15	2000	63	9.5	2	96	Tris-HCl	12	40	12	76	80	(Baskaran et al., 2018)

[AO] (Max load from Aspergillus oryzae β-galactosidase).
[KI] (Max load from Kluyveromyces lactis β-galactosidase).
[G] (From G. Stearothermophilus).
[B] (From Bacillus licheniformis).
[a] (20.08 μg/ml for 180 μl of activated magnetic CNCs (estimated by Bradford assay)).
[SF] (Temperature based on stability factor); NBA: n-butyl alcohol, CU-DES: Choline chloride (ChCl):urea(1:2)-Deep eutectic solvent; SAB: Sodium acetate buffer; DMAPP: dimethylallyl diphosphate, p-NPP: *p*-nitrophenylpalmitate; RT: Room temperature; ICT: Incubation time, RU: Reusability.

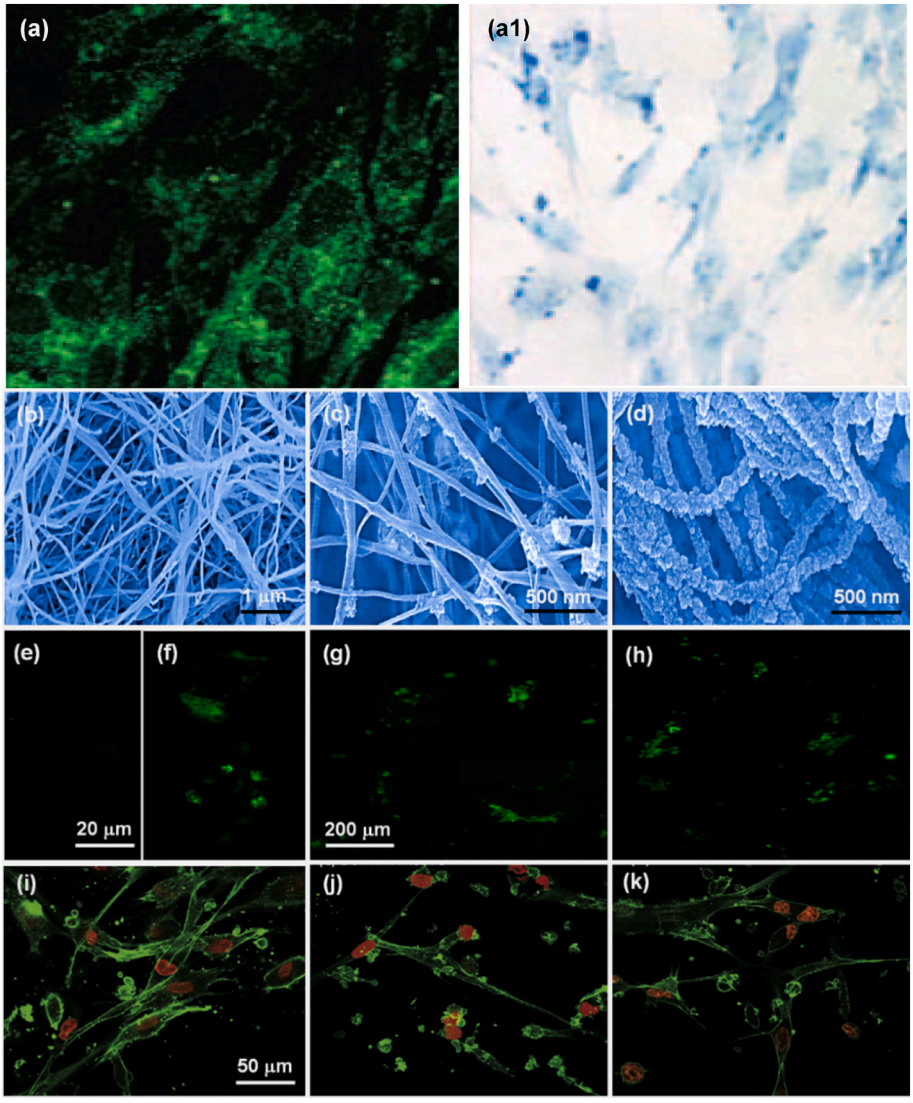

Fig. 7. a) and a1), Cells grown in culture exhibit endothelial phenotype, with the presence of von Willebrand factor (confocal microscopy, 630× magnification) (a), and positive lectin uptake (immunostaining, 100× magnification) (a1). Adapted and reprinted from Pislaru et al. (2006). with proper permission from Elsevier (Pislaru et al., 2006). SEM images of BC@Fe_3O_4 fibers. b) untreated BC. (c–d) BC treated with different iron salts concentration (ISC: 50 and 100 mM). e), Without an EMF, the BC@Fe_3O_4 could not retain circulating cells at 50 mM; f), Fe_3O_4@BC exposed to an EMF produced by two magnets facing each other at ISC of 50 mM; g), 100 mM. h), Collagen coated-BC@Fe_3O_4 with an ISC of 50 mM. HASMC cultured: i), untreated BC. (j–k), Fe_3O_4@BC with the ISC of 50 and 100 mM respectively. The green color corresponds to the F-actin cytoskeleton, and the red color to the cell nucleus of HASMC, respectively. Adapted and reprinted from Arias et al. (2018) with proper permission from Elsevier, (Arias et al., 2018).

Gd_2O_3 and MnO nanomaterials, and superparamagnetic including, Fe_3O_4, $ZnFe_2O_4$, and Fe_5C_2 nanomaterials (Ni et al., 2017). Based on the magnitude of their relaxivities r1 and r2, they can also be categorized as T1 positive and T2 negative contrast agents (Sattarahmady et al., 2016). The CSMN, as contrast agents, have extensively been employed to enhance MRI performance or efficiency through improving image contrast. Interestingly, CSMN based on poly(lactide-*co*-glycolide)/Fe_3O_4@cellulose NPs has been reported as T2-contrast agent for MRI-based cell tracking, with the particles offering the possibility of long-term MRI cell tracking experiments (Nkansah et al., 2011). Another study has reported CMC-coated Fe_3O_4 (CMC@Fe_3O_4) based MRI probe for targeting hepatocellular carcinoma with very good negative contrast, high relaxivity of 543.3 mM^{-1} s^{-1} and without any further vectorization (Sitthichai et al., 2015).

The sensitivity and reliability of MRI have improved as a result of the effect of contrast agents on the relaxation time of water protons during MRI relaxivity measurement (Leng et al., 2015). It measures the T1 and T2 relaxation times of hydrogen atom spins in tissues are called T1- or T2-weighted scans. Clinically, the effect of contrast agents depends on the longitudinal (T1) and transverse (T2) relaxation times of water protons in the human body (Li, Zhi, et al., 2016). The relaxation of water protons can be greatly influenced by a stronger local magnetic field. Fig. 8(a–b) illustrates the concept of water protons in conjunction with magnetic particles. The local magnetic field intensity of the T1 and T2 contrast materials varies with their spin phenomena, and in Fig. 8(b), it is reduced due to the presence of the T1 contrast material outside of the T2 contrast material. As a result, antiparallel spin ordering in the opposite direction of the magnetic field induced by the T2 contrast material reduces T1 contrast effect (Zhou et al., 2012). By contrast, the presence of T1 contrast material within T2 contrast material improves both of their local magnetic field strengths. Because (1) T1 contrast material can exhibits parallel spin ordering with the same direction of magnetic field induced by the T2 contrast material, and (2) T2 contrast material increases the local magnetic field strength of the T1 contrast material, resulting in a greater impact on T1 relaxation rates, and thus enhances the T1 contrast effect (Zhou et al., 2012).

Recently, a dual (T1-T2) contrast agent based on Fe_3O_4 NPs and CNC-poly citric acid has been developed for MRI application (Torkashvand et al., 2019). It has shown excellent contrast enhancement effect on both T_1 and T_2-weighted MR images with high values of r1 (13.8 mM^{-1} s^{-1}) and r2 (96.2 mM^{-1} s^{-1}) relaxivity as compared to commercial and clinical agents. The contrast of T_1- and T_2-weighted images has increased as the iron content has increased. Certainly, as iron concentrations increased: (1) the signal intensity of T_1-weighted images (brighter images) increased while T_2-weighted images (darker images) dropped significantly (Fig. 8(c)); (2) the dipole moment of this nanohybrid affects the protons of water molecules, resulting in a shorter spin-spin relaxation time (T2) and; (3) the formation of a direct coordination

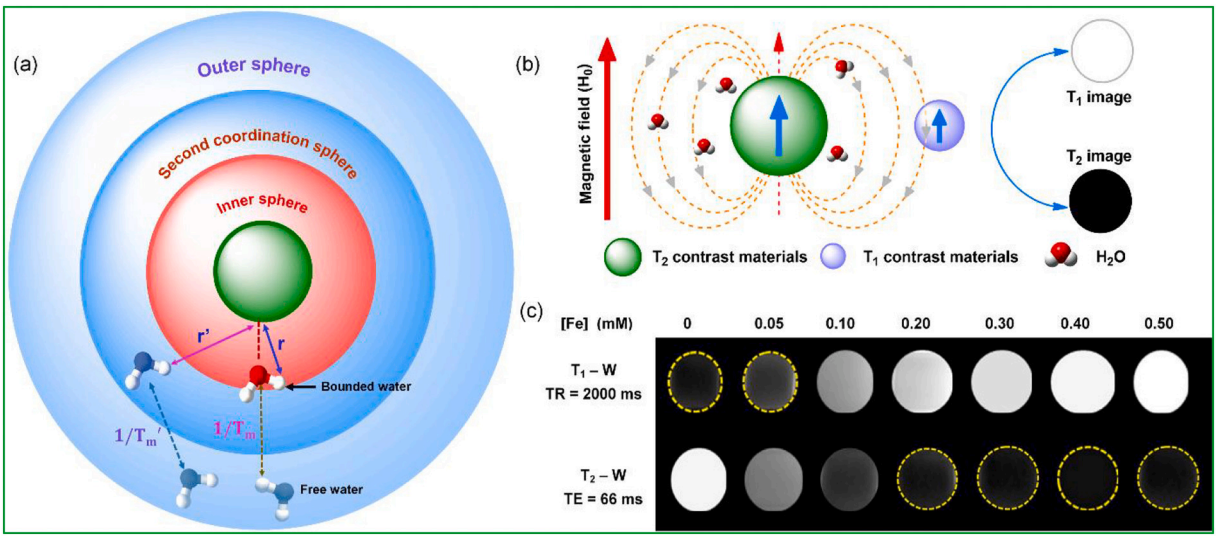

Fig. 8. Sketch of the CSMN relaxing water proton. a), (i) The inner sphere (red color), made up of carbonyl carbons and oxygen atoms, contained within the cellulose, which coordinates to the MNP and one coordinated water molecule; (ii) The distances r and r′ from MNP to H of water molecules present in an inner and second sphere (blue color); (iii) The water molecule's exchange rates of 1/Tm and 1/T′m from the bulk water to inner and second sphere respectively (Pasin et al., 2018). b), The spin phenomena between T1 and T2 contrast materials in the presence of water molecules and the respective T_1 and T_2-images. c), T_1 and T_2-weighted MRI images of CNC-poly citric acid/Fe_3O_4 at different Fe concentrations (mM) at 3.0 T where, TE = Echo time and TR = Repetition time. Adapted and reprinted from Torkashvand and Sarlak (2019) Elsevier.

bond between iron ions and water molecules shorten the longitudinal relaxation time (T1). The carboxyl and hydroxyl groups are assisted for this bond formation by absorbing more water molecules on the nano-hybrid's surface (Torkashvand et al., 2019).

Recently, CPEG coated Salep@hydrazine-Fe_3O_4 MNPs based double-layered core-shells have been reported as a negative contrast agent with r2 (81.8 mM^{-1} s^{-1}) (Hosseini et al., 2020), which is comparable to commercially available negative contrast agents such as Ferumoxtran-10, Ferumoxytol, and VSOP-C184, respectively, with r2 values of 65, 89 and 33,4 mM^{-1} s^{-1}. The toxicity of an MRI contrast agent should also be considered in addition to its ability to improve MRI images. The Fe_3O_4@DAS@CPEG used as an MRI contrast agent showed a good linear correlation between a T2 relaxation rate and a solution concentration of Fe_3O_4 (Hosseini et al., 2020). In comparison, Co—Cu doped manganese ferrite nanorods integrated CMC has also shown better as dual-modal simultaneous contrast agent for this purpose (Abbasi Pour et al., 2017). Overall, contrast agents containing (1) paramagnetic gadolinium shorten the T1 and T2 relaxation times of neighboring water protons, increasing the signal intensity of T1-weighted images while decreasing the signal intensity of T2-weighted images, and (2) transition metal ions, such as high spin MnO and superparamagnetic Fe_3O_4, have a strong effect on T2 relaxation.

5. Challenges in CSMNs developments

Although CSMNs are being attracted to advanced biomedical applications, there have been several challenges in production to date. Synthesis is a central part of these materials that should be done further in developing and processing cellulose to make them as efficient, functional, high-value-added CSMNs. Many attempts faced drawbacks and challenges in the conventional methodology, which is always reported in the literature. In particular, its incompatible nature to dissolve the cellulose in the commonly used solvents is often addressed. In this context, some disadvantages such as low thermal stability, moisture absorption, weak compatibility, and quality variations, should also be considered. The synthesis of magnetically induced BC supported nano-hybrids deteriorate the magnetic properties and limits them to be used in biomedical applications. Insufficient mechanical strength of hydroxyethyl cellulose could be overcome either by filling the polymer with NPs or suitable surface modifications to make advanced hybrid cellulose materials for medical applications. To date, the mechanical properties of these particles are also an enormous problem. In this context, fine-tuned elastic properties of magnetic BC fibrils could be achieved via distortion under magnetic field gradients for drug-delivery systems and mechano-transduction platforms. Most of these systems were formulated, evaluated, and achieved significant therapeutical effects in small animal models, but the translation of animal studies into clinical success was minimal. In furtherance, more clinical information is needed to fully understand the benefits and disadvantages of these drug carriers. In cancer therapy, the challenges include, minimize the hyperthermia ablation, controlled drug delivery, detecting malignant cells, tracking their location in the living body through in vivo imaging, and killing cancer cells while producing the least adverse side effects by stinting normal cells are playing a major role to choose the suitable components to synthesis CSMN.

6. Conclusions and prospects

Magnetic nanoparticles such as Fe_3O_4, $MnFe_2O_4$, $CoFe_2O_4$, and so on play a crucial role in biomedical applications. Over the years, cellulose and its derivatives with different functionalities and different MNPs have been used in CSMN designs. A state-of-art of CSMNs on structural details, physicomagnetic characteristics, and mechanisms has been emphasized in the present review. Their applications have been extended to different advanced areas in the biomedical field due to their unique and adjustable physicomagnetic properties, including: (1) types of cellulose. Every type of cellulose has unique attributes for instance MCC, CNC, BC, and CNF all have different physicomechanical properties and solubility. (2) size and composition of the MNPs which affect magnetic properties such as magnetization, remanence and coerciveness. (3) the shape of the CSMN. For instance, core-shell structured CSMN was found to be a promising candidate expanding the scope of many biomedical applications in stimuli-responsive drug delivery systems, and enzyme immobilization. We highlight various techniques to obtain different shapes of CSMNs and their magnetic properties concerning cellulose, MNPs, and some selective approaches to make promising homogeneous and heterogeneous cellulose solvent systems. The use of these CSMNs as support/template for stimuli-responsive drug

delivery systems, MRI, nucleic acid extraction, tissue engineering and wound healing applications in the form of a membrane, multifunctional nanocarriers, folate-conjugates, colloidal and Pickering emulsions, hydrogel beads, contrast agents, microsphere, scaffolds, hydrogel, shows that they have excellent potential characteristics for these processes.

The designs and architecture of CSMNs are still at the beginning stage of development. Therefore, cellular labeling, electromagnetic wave shielding, sensor materials, catalyst, and biocatalyst applications can be a promising field of research to explore CSMNs. Besides, with Fe_3O_4 and silver (Ag) NPs, CSMN can be used effectively for medical device disinfection, with a mixture of both magnetic and bactericidal impacts. Similarly, $CoFe_2O_4$ associated CSMN for various surface modifications of cellulose can be evaluated to check antimicrobial, biodegradable, and electromagnetic properties of a wider range of biomedical applications. Thus, for those who intend to experiment with the surface functionality of cellulose, there are many more opportunities for the synthesis of novel nanohybrids particularly in the aforementioned biomedical application using CSMN. However, the key issue that should be noted is the biocompatibility of the CSMNs.

List of abbreviations

BC	Bacterial Cellulose
BET	Brunauer-Emmett-Teller
BTCA	1,2,3,4-butanetetracarboxylic acid
CAC	Cellulose-Activated Carbon
COF	Cobalt Ferrite
CMC	Carboxymethyl Cellulose
CTNR	Cationic Nanocarrier
CCC	Calcium Chloride Coagulation
CAL	Candida Antarctica lipase
CTMB	Cellulose Tris-(4-methylbenzoate)
CBD	Cellulose-Binding Domain
CU	Choline-chloride Urea
CSSNF	Core-Shell Super Paramagnetic Nanofluids
CR	Cumulative Release
CD	Cyclodextrin
Cur-MFCMC	Curcumin loaded $MnFe_2O_4$–CMC
β-CD	β-cyclodextrin
DES	Deep Eutectic Solvent
DP	Degree of Polymerization
DAS	Dialdehyde Salep
DMAPP	Dimethylallyl Diphosphate
DOX	Doxorubicin
DD	Draw Direction
EDC	N-(3-dimethyl aminopropyl)-N′-ethyl carborodiimidehydrochloride
EISA	Evaporation-Induced Self-Assembly
EMF	External Magnetic Field
FE-SEM	Field Emission Scanning Electron Microscope
FC	Folate Conjugate
FC-MCMC-NV	FC conjugated CMC-based magnetic nanovector
GO	Glucose Oxidase
GA	Glutaraldehyde
GPa	GigaPascal
HRTEM	High-Resolution Transmission Electron Microscope
H_C	Higher Coercivity
HASMC	Human Aortic Smooth Muscle Cells
HA	Hydroxyapatite
HPMC	Hydroxypropyl Methylcellulose
ι-Car	i-carrageenan
ILs	Ionic Liquids
ICT	Incubation time
IAA	Indole-3-Acetic Acid
LbL	Layer-by-Layer
MCNAS	Core−Shell Structured Magnetic Cellulose Microsphere
MHT	Magnetic Hyperthermia
MNPs	Magnetic Nanoparticles
MRI	Magnetic Resonance Imaging
MT	Magnetotherapy
mRNA	Messenger RNA
MTX	Methotrexate: (N-[4[[2,4-diamino-6-pyridinyl)methyl] methyl-amino]benzoil]-L-glutamic acid))
MTT	3-(4,5-dimethylthiazol-2-yl)-2,5-diphenyltetrazolium bromide
MCC	Microcrystalline Cellulose
MPa	MegaPascal
MHAB	Magnetic HA hybrid beads
M_s	Saturation Magnetization
NBA	n-butyl alcohol
NHS	N-Hydroxysuccinimide
PE	Pickering Emulsion
PESC	PE-based Smart Carriers
PEP	Polyelectrolytes Protamine
PEG	Polyethylene Glycol
CPEGs	Polyethylene Glycol Functionalized CMCs
PVA	Polyvinyl Alcohol
PEI	Polyethyleneimine
PEEK	poly(ether ether ketone)
p-NPP	*p*-nitrophenylpalmitate
PCMC	Pineapple Peel Carboxymethyl Cellulose
PMADQUAT	Dimethyl aminoethyl methacrylate quaternary ammonium alkyl halide
RU	Reusability
RT	Room Temperature
SEM	Scanning Electron Microscope
SPNAE	Solid-Phase Nucleic Acid Extraction
SAB	Sodium Acetate Buffer
SRDD	Stimuli-Responsive Drug Delivery Systems
SA	Streptavidin
SR	Swelling Rate
TEVG	Tissue-Engineered Vascular Graft
TEM	Transmission Electron Microscope
TEMPO	2,2,6,6-tetramethylpiperidine-1-oxyl radical
ZFC	Zero-Field-Cooled

CRediT authorship contribution statement

Mhd. Abd. Cader. Mhd. Haniffa: Conceptualization, Data curation, Writing-Original Draft, Preparation of Figures and Tables. **Khadija Munawar**: Data curation, and Figures setting. **Ching Yern Chee**: Project administration and Resources. **Sumit Pramanik**: Data curation, Review and editing manuscript. **Ahmed Halilu**: Critical review and editing manuscript. **Hazlee Azil Illias**: Project administration and Resources. **Rajendram Senthilnithy**: Review and editing manuscript. **Kariyawasam Ranaweerage Ranjith Mahanama**: Critical Review and editing manuscript. **Ashis Tripathy**: Data curation and Review. **Muhammad Rizwan**: Data curation and Review. **Mohd Fahmi Azman**: Data curation and Review.

Competing interests

The authors declare no competing interests.

Acknowledgements

Authors are grateful to the Faculty of Engineering, University of Malaya, for financial support through grant no: HIR (H-16001-D00048), Faculty Research Grant (GPF077A-2018) and Impact-Oriented Interdisciplinary Research Grant (IIRG001-2020IISS). Nippon Sheet Glass Foundation Research Grant (NSGF-IF007-2021) is also gratefully

acknowledged.

Appendix A. Supplementary data

Supplementary data to this article can be found online at https://doi.org/10.1016/j.carbpol.2021.118136.

References

Abbasi Pour, S., Shaterian, H. R., Afradi, M., & Yazdani-Elah-Abadi, A. (2017). Carboxymethyl cellulose (CMC)-loaded Co-Cu doped manganese ferrite nanorods as a new dual-modal simultaneous contrast agent for magnetic resonance imaging and nanocarrier for drug delivery system. *Journal of Magnetism and Magnetic Materials, 438*, 85–94.

Abbasian, M., Hasanzadeh, P., Mahmoodzadeh, F., & Salehi, R. (2019). Novel cationic cellulose-based nanocomposites for targeted delivery of methotrexate to breast cancer cells. *Journal of Macromolecular Science, Part A, 57*(2), 99–115.

Abou Hammad, A. B., Abd El-Aziz, M. E., Hasanin, M. S., & Kamel, S. (2019). A novel electromagnetic biodegradable nanocomposite based on cellulose, polyaniline, and cobalt ferrite nanoparticles. *Carbohydrate Polymers, 216*, 54–62.

Aguilar, N. M., Arteaga-Cardona, F., de Anda Reyes, M. E., Gervacio-Arciniega, J. J., & Salazar-Kuri, U. (2019). Magnetic bioplastics based on isolated cellulose from cotton and sugarcane bagasse. *Materials Chemistry and Physics, 238*, 121921.

Ahmad, A., Mubarak, N., Jannat, F., Ashfaq, T., Santulli, C., Rizwan, M., … Hussain, S. (2021). A critical review on the synthesis of natural sodium alginate based composite materials: An innovative biological polymer for biomedical delivery applications. *Processes, 9*, 137.

Ahmad, H. (2021). Celluloses as support materials for antibacterial agents: A review. *Cellulose*, 1–47.

Alahmadi, N. S., Betts, J. W., Cheng, F., Francesconi, M. G., Kelly, S. M., Kornherr, A., … Wadhawan, J. D. (2017). Synthesis and antibacterial effects of cobalt–cellulose magnetic nanocomposites. *RSC Advances, 7*(32), 20020–20026.

Alatawi, F. S., Monier, M., & Elsayed, N. H. (2018). Amino functionalization of carboxymethyl cellulose for efficient immobilization of urease. *International Journal of Biological Macromolecules, 114*, 1018–1025.

Alekseeva, O. V., Rodionova, A. N., Bagrovskaya, N. A., Agafonov, A. V., & Noskov, A. V. (2017). Hydroxyethylcellulose/bentonite/magnetite hybrid materials: Structure, physicochemical properties, and antifungal activity. *Cellulose, 24*(4), 1825–1836.

An, X., Cheng, D., Dai, L., Wang, B., Ocampo, H. J., Nasrallah, J., … Ni, Y. (2017). Synthesis of nano-fibrillated cellulose/magnetite/titanium dioxide (CNF@Fe_3O_4@TNP) nanocomposites and their application in the photocatalytic hydrogen generation. *Applied Catalysis B: Environmental, 206*, 53–64.

Arias, S. L., Shetty, A., Devorkin, J., & Allain, J. P. (2018). Magnetic targeting of smooth muscle cells in vitro using a magnetic bacterial cellulose to improve cell retention in tissue-engineering vascular grafts. *Acta Biomaterialia, 77*, 172–181.

Asencio, C., Chatterjee, A., & Hentze, M. W. (2018). Silica-based solid-phase extraction of cross-linked nucleic acid–bound proteins. *Life Science Alliance, 1*(3).

Azarmanesh, M., Dejam, M., Azizian, P., Yesiloz, G., Mohamad, A. A., & Sanati-Nezhad, A. (2019). Passive microinjection within high-throughput microfluidics for controlled actuation of droplets and cells. *Scientific Reports, 9*(1), 1–12.

Bandikari, R., Qian, J., Baskaran, R., Liu, Z., & Wu, G. (2018). Bio-affinity mediated immobilization of lipase onto magnetic cellulose nanospheres for high yield biodiesel in one time addition of methanol. *Bioresource Technology, 249*, 354–360.

Bardajee, G. R., Hooshyar, Z., Asli, M. J., Shahidi, F. E., & Dianatnejad, N. (2014). Synthesis of a novel supermagnetic iron oxide nanocomposite hydrogel based on graft copolymerization of poly ((2-dimethylamino) ethyl methacrylate) onto salep for controlled release of drug. *Materials Science Engineering: C, 36*, 277–286.

Bart, J., Tiggelaar, R., Yang, M., Schlautmann, S., Zuilhof, H., & Gardeniers, H. (2009). Room-temperature intermediate layer bonding for microfluidic devices. *Lab on a Chip, 9*(24), 3481–3488.

Baskaran, R., Bandikari, R., Zuo, W., Qian, J., & Liu, Z. (2018). Enhanced thermostability of halo-tolerant glutaminase from Bacillus licheniformis ATCC 14580 by immobilization onto nano magnetic cellulose sheet and its application in production of glutamic acid. *International Journal of Biological Macromolecules, 119*, 1256–1263.

Bergfeld, A. K., Pearce, O. M., Diaz, S. L., Pham, T., & Varki, A. (2012). Metabolism of vertebrate amino sugars with N-glycolyl groups: Elucidating the intracellular fate of the non-human sialic acid N-glycolylneuraminic acid. *Journal of Biological Chemistry, 287*(34), 28865–28881.

Biliuta, G., & Coseri, S. (2016). Magnetic cellulosic materials based on TEMPO-oxidized viscose fibers. *Cellulose, 23*(6), 3407–3415.

Biliuta, G., Sacarescu, L., Socoliuc, V., Iacob, M., Gheorghe, L., Negru, D., & Coseri, S. (2017). Carboxylated polysaccharides decorated with ultrasmall magnetic nanoparticles with antibacterial and MRI properties. *Macromolecular Chemistry and Physics, 218*(10).

Bullard, K. K., Srinivasarao, M., & Gutekunst, W. R. (2020). Modification of cellulose nanocrystal surface chemistry with diverse nucleophiles for materials integration. *Journal of Materials Chemistry A, 8*, 18024–18031.

Cai, J., & Zhang, L. (2005). Rapid dissolution of cellulose in LiOH/urea and NaOH/urea aqueous solutions. *Macromolecular Bioscience, 5*(6), 539–548.

Cao, S.-L., Xu, H., Lai, L.-H., Gu, W.-M., Xu, P., Xiong, J., … Lou, W.-Y. (2017). Magnetic ZIF-8/cellulose/Fe_3O_4 nanocomposite: preparation, characterization, and enzyme immobilization. *Bioresources and Bioprocessing, 4*(1), 56.

Cao, S.-L., Xu, H., Li, X.-H., Lou, W.-Y., & Zong, M.-H. (2015). Papain@magnetic nanocrystalline cellulose nanobiocatalyst: A highly efficient biocatalyst for dipeptide biosynthesis in deep eutectic solvents. *ACS Sustainable Chemistry & Engineering, 3*(7), 1589–1599.

Cardoso, V. F., Francesko, A., Ribeiro, C., Banobre-Lopez, M., Martins, P., & Lanceros-Mendez, S. (2018). Advances in magnetic nanoparticles for biomedical applications. *Advanced Healthcare Materials, 7*(5), 1700845.

Carvalho, S. M., Leonel, A. G., Mansur, A. A. P., Carvalho, I. C., Krambrock, K., & Mansur, H. S. (2019). Bifunctional magnetopolymersomes of iron oxide nanoparticles and carboxymethylcellulose conjugated with doxorubicin for hyperthermo-chemotherapy of brain cancer cells. *Biomaterials Science, 7*(5), 2102–2122.

Chen, D., Song, X., Wang, K., Guo, C., Yu, Y., Fan, H., & Zhao, F. (2017). Design and evaluation of dual CD44 receptor and folate receptor-targeting double-smart pH-response multifunctional nanocarrier. *Journal of Nanoparticle Research, 19*(12), 1–11.

Chen, L., Berry, R. M., & Tam, K. C. (2014). Synthesis of β-cyclodextrin-modified cellulose nanocrystals (CNCs)@Fe_3O_4@SiO_2 superparamagnetic nanorods. *ACS Sustainable Chemistry & Engineering, 2*(4), 951–958.

Chen, Q., Zheng, J., Yang, Q., Dang, Z., & Zhang, L. (2019). Insights into the glyphosate adsorption behavior and mechanism by a $MnFe_2O_4$@cellulose-activated carbon magnetic hybrid. *ACS Applied Materials & Interfaces, 11*(17), 15478–15488.

Chen, S., Zhao, X., Chen, J., Chen, J., Kuznetsova, L., Wong, S. S., & Ojima, I. (2010). Mechanism-based tumor-targeting drug delivery system. Validation of efficient vitamin receptor-mediated endocytosis and drug release. *Bioconjugate Chemistry, 21*(5), 979–987.

Chybczyńska, K., Markiewicz, E., Grząbka-Zasadzińska, A., & Borysiak, S. (2019). Dielectric, magnetic, and mechanical properties of composites consisting of biopolymer chitosan matrix and hybrid spinel/cellulose filler. *Ceramics International, 45*(7), 9468–9476.

Dai, H., Zhang, H., Ma, L., Zhou, H., Yu, Y., Guo, T., … Huang, H. (2019). Green pH/magnetic sensitive hydrogels based on pineapple peel cellulose and polyvinyl alcohol: Synthesis, characterization and naringin prolonged release. *Carbohydrate Polymers, 209*, 51–61.

Das, R., Kim, N. P., Attanayake, S. B., Phan, M.-H., & Srikanth, H. (2021). Role of magnetic anisotropy on the hyperthermia efficiency in spherical $Fe_{3-x}Co_xO_4$ (x = 0–1) nanoparticles. *Applied Sciences, 11*(3).

Davarpanah, A. M., Rahdar, A., Dastnae, M. A., Zeybek, O., & Beyzaei, H. (2019). (1-x) $BaFe_{12}O_{19}$/x$CoFe_2O_4$ hard/soft magnetic nanocomposites: Synthesis, physical characterization, and antibacterial activities study. *Journal of Molecular Structure, 1175*, 445–449.

Dhahri, A., Jaoua-Bahloul, H., Baouab, M. H. V., Luneau, D., & Beyou, E. (2018). Magnetic properties of cellulose-grafted reduced graphite oxide decorated with Ni nanoparticles. *Polymer Engineering & Science, 58*(9), 1630–1635.

Dhar, P., Kumar, A., & Katiyar, V. (2016). Magnetic cellulose nanocrystal based anisotropic polylactic acid nanocomposite films: Influence on electrical, magnetic, thermal, and mechanical properties. *ACS Applied Materials & Interfaces, 8*(28), 18393–18409.

Dimke, H., Larsen, S. L., Skov, M. N., Larsen, H., Hartmeyer, G. N., & Moeller, JB. (2021). Phenol-chloroform-based RNA purification for detection of SARS-CoV-2 by RT-qPCR: Comparison with automated systems. *PLoS One, 16*(2), Article e0247524. https://doi.org/10.1371/journal.pone.0247524

Drout, R. J., Robison, L., & Farha, O. K. (2019). Catalytic applications of enzymes encapsulated in metal–organic frameworks. *Coordination Chemistry Reviews, 381*, 151–160.

Du, K., Liu, X., Li, S., Qiao, L., & Ai, H. (2018). Synthesis of Cu^{2+} chelated cellulose/magnetic hydroxyapatite particles hybrid beads and their potential for high specific adsorption of histidine-rich proteins. *ACS Sustainable Chemistry & Engineering, 6*(9), 11578–11586.

Elisseeff, J. (2008). Structure starts to gel. *Nature Materials, 7*(4), 271–273.

Elumalai, R., Patil, S., Maliyakkal, N., Rangarajan, A., Kondaiah, P., & Raichur, A. M. (2015). Protamine-carboxymethyl cellulose magnetic nanocapsules for enhanced delivery of anticancer drugs against drug resistant cancers. *Nanomedicine, 11*(4), 969–981.

Emaus, M. N., Varona, M., Eitzmann, D. R., Hsieh, S.-A., Zeger, V. R., & Anderson, J. L. (2020). Nucleic acid extraction: Fundamentals of sample preparation methodologies, current advancements, and future endeavors. *TrAC Trends in Analytical Chemistry, 130*, Article 115985.

Engel, B. J., Grindel, B. J., Gray, J. P., & Millward, S. W. (2020). Purification of poly-dA oligonucleotides and mRNA-protein fusions with dT25-OAS resin. *Bioorganic Medicinal Chemistry Letters, 30*(4), 126934.

Eslahi, N., Mahmoodi, A., Mahmoudi, N., Zandi, N., & Simchi, A. (2020). Processing and properties of nanofibrous bacterial cellulose-containing polymer composites: A review of recent advances for biomedical applications. *Polymer Reviews, 60*(1), 144–170.

Esser, K.-H., Marx, W. H., & Lisowsky, T. (2006). maxXbond: First regeneration system for DNA binding silica matrices. *Nature Methods, 3*(1), i–ii.

Ewulonu, C. M., Liu, X., Wu, M., & Yong, H. (2019). Lignin-containing cellulose nanomaterials: A promising new nanomaterial for numerous applications. *Journal of Bioresources and Bioproducts, 4*(1), 3–10.

Fantechi, E., Innocenti, C., Albino, M., Lottini, E., & Sangregorio, C. (2015). Influence of cobalt doping on the hyperthermic efficiency of magnetite nanoparticles. *Journal of Magnetism Magnetic Materials, 380*, 365–371.

Furlan, D. M., Morgado, D. L., Oliveira, A. J. A. D., Faceto, Â. D., Moraes, D. A. D., Varanda, L. C., & Frollini, E. (2019). Sisal cellulose and magnetite nanoparticles: Formation and properties of magnetic hybrid films. *Journal of Materials Research and Technology, 8*(2), 2170–2179.

Galateanu, B., Bunea, M. C., Stanescu, P., Vasile, E., Casarica, A., Iovu, H., … Costache, M. (2015). In vitro studies of bacterial cellulose and magnetic nanoparticles smart nanocomposites for efficient chronic wounds healing. *Stem Cells International, 2015*, 195096.

Galland, S., Andersson, R. L., Strom, V., Olsson, R. T., & Berglund, L. A. (2014). Strong and moldable cellulose magnets with high ferrite nanoparticle content. *ACS Applied Material & Interfaces, 6*(22), 20524–20534.

Ganguly, K., Patel, D. K., Dutta, S. D., Shin, W.-C., & Lim, K.-T. (2020). Stimuli-responsive self-assembly of cellulose nanocrystals (CNCs): Structures, functions, and biomedical applications. *International Journal of Biological Macromolecules, 155*, 456–469.

Gao, Z., Zhang, Q., Cao, Y., Pan, P., Bai, F., & Bai, G. (2009). Preparation of novel magnetic cellulose microspheres via cellulose binding domain-streptavidin linkage and use for mRNA isolation from eukaryotic cells and tissues. *Chromatography A, 1216*(45), 7670–7676.

Garg, A., Goel, S., Kumari, N., Dubey, A., Prasad, N. E., & Tyagi, S. (2020). Development of $SrFe_{12}O_{19}/Ti_3SiC_2$ composites for enhanced microwave absorption. *Journal of Electronic Materials, 49*(3), 2233–2241.

Ge, Y., Zhang, Y., Xia, J., Ma, M., He, S., Nie, F., & Gu, N. (2009). Effect of surface charge and agglomerate degree of magnetic iron oxide nanoparticles on KB cellular uptake in vitro. *Colloids Surfaces B: Biointerfaces, 73*(2), 294–301.

Gennari, A., Führ, A. J., Volpato, G., & de Souza, C. F. V. (2020). Magnetic cellulose: Versatile support for enzyme immobilization-A review. *Carbohydrate Polymers, 246*, Article 116646.

Gennari, A., Mobayed, F. H., Da Rolt Nervis, B., Benvenutti, E. V., Nicolodi, S., da Silveira, N. P., … Volken de Souza, C. F. (2019). Immobilization of beta-galactosidases on magnetic nanocellulose: Textural, morphological, magnetic, and catalytic properties. *Biomacromolecules, 20*(6), 2315–2326.

Ghosh, T., Teramoto, Y., & Katiyar, V. (2019). Influence of nontoxic magnetic cellulose nanofibers on chitosan based edible nanocoating: A candidate for improved mechanical, thermal, optical, and texture properties. *Agriculture Food Chemistry, 67*(15), 4289–4299.

Green, M. R., & Sambrook, J. (2018). A single-step method for the simultaneous preparation of DNA, RNA, and protein from cells and tissues. *Cold Spring Harbor Protocols, 2018*(1) (pdb. prot093500).

Guo, X., Xue, L., Lv, W., Liu, Q., Li, R., Li, Z., & Wang, J. (2015). Facile synthesis of magnetic carboxymethylcellulose nanocarriers for pH-responsive delivery of doxorubicin. *New Journal of Chemistry, 39*(9), 7340–7347.

Guo, Y., Chen, X., Zhang, X., Pu, S., Zhang, X., Yang, C., & Li, D. (2018). Comparative studies on ZIF-8 and SiO_2 nanoparticles as carrier for immobilized β-glucosidase. *Journal of Molecular Catalyst, 459*, 1–7.

Halilu, A., Ali, T. H., Atta, A. Y., Sudarsanam, P., Bhargava, S. K., & Abd Hamid, S. B. (2016). Highly selective hydrogenation of biomass-derived furfural into furfuryl alcohol using a novel magnetic nanoparticles catalyst. *Energy & Fuels, 30*(3), 2216–2226.

Halilu, A., Hussein Ali, T., Sudarsanam, P., & Bhargava, S. K. (2019). Synthesis of fuel grade molecules from hydroprocessing of biomass-derived compounds catalyzed by magnetic Fe (NiFe) O4-SiO_2 nanoparticles. *Symmetry, 11*(4), 524.

Haniffa, M. A. C. M., Ching, Y. C., Illias, H. A., Munawar, K., Ibrahim, S., Nguyen, D. H., & Chuah, C. H. (2020). Cellulose supported promising magnetic sorbents for magnetic solid-phase extraction: A review. *Carbohydrate Polymers, 253*, 117245.

Hao, R., Xing, R., Xu, Z., Hou, Y., Gao, S., & Sun, S. (2010). Synthesis, functionalization, and biomedical applications of multifunctional magnetic nanoparticles. *Advanced Materials, 22*(25), 2729–2742.

He, X., Liang, C., Liu, Q., & Xu, Z. (2019). Magnetically responsive Janus nanoparticles synthesized using cellulosic materials for enhanced phase separation in oily wastewaters and water-in-crude oil emulsions. *Chemical Engineering Journal*, 378.

Heise, K., Delepierre, G., King, A., Kostiainen, M., Zoppe, J., Weder, C., & Kontturi, E. (2020). Chemical modification of cellulose nanocrystal reducing end groups. *Angewandte Chemie, 60*(1), 66–87.

Hosseini, S. H., Zohreh, N., Karimi, N., Gaeini, N., Alipour, S., Seidi, F., & Gholipour, N. (2020). Magnetic nanoparticles double wrapped into cross-linked salep/PEGylated carboxymethyl cellulose; a biocompatible nanocarrier for pH-triggered release of doxorubicin. *International Journal of Biological Macromolecules, 158*, 994–1006.

Hou, L., Udangawa, W. M. R. N., Pochiraju, A., Dong, W., Zheng, Y., Linhardt, R. J., & Simmons, T. J. (2016). Synthesis of heparin-immobilized, magnetically addressable cellulose nanofibers for biomedical applications. *ACS Biomaterials Science & Engineering, 2*(11), 1905–1913.

Huang, T., Song, P., Jiang, L., Peng, Y., Feng, S., & Wang, J. (2016). Electrospinning of magnetic cellulose tris-(4-methylbenzoate) microparticles for enantioselective adsorption of racemic drug. *Electrophoresis, 37*(14), 2050–2053.

Jaetao, J. E., Butler, K. S., Adolphi, N. L., Lovato, D. M., Bryant, H. C., Rabinowitz, I., … Bergemann, C. (2009). Enhanced leukemia cell detection using a novel magnetic needle and nanoparticles. *Cancer Research, 69*(21), 8310–8316.

Kanagarajan, S. V., & Thiyagarajan, D. (2018). Carboxymethyl cellulose-functionalised magnetic nanocarriers for pH responsive delivery of Curcumin in cancer therapy. *Materials Research Express, 6*(1), Article 016105.

Kang, M. H., Yoo, H. J., Kwon, Y. H., Yoon, H. Y., Lee, S. G., Kim, S. R., … Choi, Y. W. (2015). Design of multifunctional liposomal nanocarriers for folate receptor-specific intracellular drug delivery. *Molecular Pharmaceutics, 12*(12), 4200–4213.

Kanikireddy, V., Varaprasad, K., Jayaramudu, T., Karthikeyan, C., & Sadiku, R. (2020). Carboxymethyl cellulose-based materials for infection control and wound healing: A review. *International Journal of Biological Macromolecules, 164*(1), 963–975.

Karzar Jeddi, M., & Mahkam, M. (2019). Magnetic nano carboxymethyl cellulose-alginate/chitosan hydrogel beads as biodegradable devices for controlled drug delivery. *International Journal of Biological Macromolecules, 135*, 829–838.

Kazenwadel, F., Wagner, H., Rapp, B. E., & Franzreb, M. (2015). Optimization of enzyme immobilization on magnetic microparticles using 1-ethyl-3-(3-dimethylamino-propyl)carbodiimide (EDC) as a crosslinking agent. *Analytical Methods, 7*(24), 10291–10298.

Kim, E.-S., Enkhzaya, G., Hwang, H.-S., Han, J.-H., Kim, C.-S., Shin, J.-W., Yoon, Y.-R., & Kim, N.-Y. (2021). Highly efficient transfection effect of transdermal drug delivery via skin by hybrid bipolar arc plasma stimulation and dual pulse electroporation technique. *IEEE Access, 9*, 24071–24078.

Lei, L., Bai, Y., Li, Y., Yi, L., Yang, Y., & Xia, C. (2009). Study on immobilization of lipase onto magnetic microspheres with epoxy groups. *Journal of Magnetism and Magnetic Materials, 321*(4), 252–258.

Leng, J., Li, J., Ren, J., Deng, L., & Lin, C. (2015). Star–block copolymer micellar nanocomposites with Mn, Zn-doped nano-ferrite as superparamagnetic MRI contrast agent for tumor imaging. *Materials Letters, 152*, 185–188.

Leonel, A. G., Mansur, H. S., Mansur, A. A., Caires, A., Carvalho, S. M., Krambrock, K., … Ardisson, J. D. (2019). Synthesis and characterization of iron oxide nanoparticles/carboxymethyl cellulose core-shell nanohybrids for killing cancer cells in vitro. *International Journal of Biological Macromolecules, 132*, 677–691.

Li, A. Y., Kaushik, M., Li, C.-J., & Moores, A. (2016). Microwave-assisted synthesis of magnetic carboxymethyl cellulose-embedded Ag–Fe_3O_4 nanocatalysts for selective carbonyl hydrogenation. *ACS Sustainable Chemistry & Engineering, 4*(3), 965–973.

Li, B., Zhang, Q., Pan, Y., Li, Y., Huang, Z., Li, M., & Xiao, H. (2020). Functionalized porous magnetic cellulose/Fe_3O_4 beads prepared from ionic liquid for removal of dyes from aqueous solution. *International Journal of Biological Macromolecules, 163*, 309–316.

Li, F., Zhi, D., Luo, Y., Zhang, J., Nan, X., Zhang, Y., … Liang, G. (2016). Core/shell Fe_3O_4/Gd_2O_3 nanocubes as T1–T2 dual modal MRI contrast agents. *Nanoscale, 8*(25), 12826–12833.

Li, J., Wang, Y., Sun, Y., Ding, C., Lin, Y., Sun, W., & Luo, C. (2017). A novel ionic liquid functionalized graphene oxide supported gold nanoparticle composite film for sensitive electrochemical detection of dopamine. *RSC Advances, 7*(4), 2315–2322.

Li, X., Feng, Q., Lu, K., Huang, J., Zhang, Y., Hou, Y., Qiao, H., Li, D., & Wei, Q. (2021). Encapsulating enzyme into metal-organic framework during in-situ growth on cellulose acetate nanofibers as self-powered glucose biosensor. *Biosensors & Bioelectronics, 171*, Article 112690.

Li, X., Li, D., Zhang, Y., Lv, P., Feng, Q., & Wei, Q. (2020). Encapsulation of enzyme by metal-organic framework for single-enzymatic biofuel cell-based self-powered biosensor. *Nano Energy, 68*, 104308.

Li, X., Wei, J., Aifantis, K. E., Fan, Y., Feng, Q., Cui, F. Z., & Watari, F. (2016). Current investigations into magnetic nanoparticles for biomedical applications. *Journal of Biomedical Materials Research Part A, 104*(5), 1285–1296.

Li, Z., Lu, S., Jin, J., & Wang, T. (2018). Preparation of a new cellulose magnetic molecularly imprinted polymer micro-spheres to extract and analyze the indole-3-acetic acid in plant tissues. *Journal of Chromatography B: Analytical Technologies in the Biomedical and Life Sciences, 1092*, 343–349.

Lian, T., & Ho, R. J. (2001). Trends and developments in liposome drug delivery systems. *Journal of Pharmaceutical Sciences, 90*(6), 667–680.

Liang, Y., Liu, J., Wang, L., Wan, Y., Shen, J., & Bai, Q. (2019). Metal affinity-carboxymethyl cellulose functionalized magnetic graphene composite for highly selective isolation of histidine-rich proteins. *Talanta, 195*, 381–389.

Liao, J., & Huang, H. (2020). Review on magnetic natural polymer constructed hydrogels as vehicles for drug delivery. *Biomacromolecules, 21*(7), 2574–2594.

Limaye, M. V., Sahoo, P. K., Shirolkar, M., Singh, S. B., Khare, A., Shao, Y. C., … Pong, W. F. (2019). Fabrication and 3D patterning of bio-composite consisting of carboxymethylated cellulose nanofibers and cobalt ferrite nanoparticles. *ChemistrySelect, 4*(14), 4416–4421.

Lin, F., Zheng, J., Guo, W., Zhu, Z., Wang, Z., Dong, B., Lin, C., Huang, B., & Lu, B. (2019). Smart cellulose-derived magnetic hydrogel with rapid swelling and deswelling properties for remotely controlled drug release. *Cellulose, 26*(11), 6861–6877.

Liu, C., Saeki, D., & Matsuyama, H. (2017). A novel strategy to immobilize enzymes on microporous membranes via dicarboxylic acid halides. *RSC Advance., 7*(76), 48199–48207.

Liu, H., Zhao, F., Jin, C. E., Koo, B., Lee, E. Y., Zhong, L., … Shin, Y. (2018). Large instrument-and detergent-free assay for ultrasensitive nucleic acids isolation via binary nanomaterial. *Analytical Chemistry, 90*(8), 5108–5115.

Liu, S., Zhou, J., & Zhang, L. (2011). In situ synthesis of plate-like Fe_2O_3 nanoparticles in porous cellulose films with obvious magnetic anisotropy. *Cellulose, 18*(3), 663–673.

Liu, W., Du, H., Zhang, M., Liu, K., Liu, H., Xie, H., … Si, C. (2020). Bacterial cellulose-based composite scaffolds for biomedical applications: A review. *ACS Sustainable Chemistry & Engineering, 8*(20), 7536–7562.

Liu, Y., Berrido, A. M., Hua, Z.-C., Tse-Dinh, Y.-C., & Leng, F. (2017). Biochemical and biophysical properties of positively supercoiled DNA. *Biophysical Chemistry, 230*, 68–73.

Lizundia, E., Maceiras, A., Vilas, J., Martins, P., & Lanceros-Mendez, S. (2017). Magnetic cellulose nanocrystal nanocomposites for the development of green functional materials. *Carbohydrate Polymers, 175*, 425–432.

Low, L. E., Tan, L. T., Goh, B. H., Tey, B. T., Ong, B. H., & Tang, S. Y. (2019). Magnetic cellulose nanocrystal stabilized Pickering emulsions for enhanced bioactive release and human colon cancer therapy. *International Journal of Biological Macromolecules, 127*, 76–84.

Low, L. E., Tey, B. T., Ong, B. H., & Tang, S. Y. (2018). Unravelling pH-responsive behaviour of Fe_3O_4@CNCs-stabilized Pickering emulsions under the influence of magnetic field. *Polymer, 141*, 93–101.

Lu, Y., Wang, Y., Liu, L., & Yuan, W. (2017). Environmental-friendly and magnetic/silanized ethyl cellulose sponges as effective and recyclable oil-absorption materials. *Carbohydrate Polymers, 173*, 422–430.
Luo, H., Cha, R., Li, J., Hao, W., Zhang, Y., & Zhou, F. (2019). Advances in tissue engineering of nanocellulose-based scaffolds: A review. *Carbohydrate Polymers, 224*, 115144.
Luo, X., & Zhang, L. (2010). Immobilization of penicillin G acylase in epoxy-activated magnetic cellulose microspheres for improvement of biocatalytic stability and activities. *Biomacromolecules, 11*(11), 2896–2903.
Magnani, M., & Rossi, L. (2014). Approaches to erythrocyte-mediated drug delivery. *Expert Opinion on Drug Delivery, 11*(5), 677–687.
Mahalunkar, S., Yadav, A. S., Gorain, M., Pawar, V., Braathen, R., Weiss, S., … Kundu, G. C. (2019). Functional design of pH-responsive folate-targeted polymer-coated gold nanoparticles for drug delivery and in vivo therapy in breast cancer. *International Journal of Nanomedicine, 14*, 8285–8302.
Malakootikhah, J., Rezayan, A. H., Negahdari, B., Nasseri, S., & Rastegar, H. (2017). Glucose reinforced Fe_3O_4@cellulose mediated amino acid: Reusable magnetic glyconanoparticles with enhanced bacteria capture efficiency. *Carbohydrate Polymers, 170*, 190–197.
Mansur, A. A. P., Carvalho, S. M., Lobato, Z. I. P., Leite, M. F., Cunha, A. D. S., Jr., & Mansur, H. S. (2018). Design and development of polysaccharide-doxorubicin-peptide bioconjugates for dual synergistic effects of integrin-targeted and cell-penetrating peptides for cancer chemotherapy. *Bioconjugate Chemistry, 29*(6), 1973–2000.
Marti-Mestres, G., Nielloud, F., & technology. (2002). Emulsions in health care applications—An overview. *Journal of Dispersion Science, 23*(1–3), 419–439.
Matos, R. J. R., Chaparro, C. I. P., Silva, J. C., Valente, M. A., Borges, J. P., & Soares, P. I. P. (2018). Electrospun composite cellulose acetate/iron oxide nanoparticles non-woven membranes for magnetic hyperthermia applications. *Carbohydrate Polymers, 198*, 9–16.
Meng, J., Wang, Y., Zhou, Y., Chen, J., Wei, X., Ni, R., … Xu, F. (2020). A composite consisting of a deep eutectic solvent and dispersed magnetic metal-organic framework (type UiO-66-NH_2) for solid-phase extraction of RNA. *Microchimica Acta, 187*(1), 58.
Mhd Haniffa, M. A. C., Ching, Y. C., Chuah, C. H., Yong Ching, K., Nazri, N., Abdullah, L. C., & Nai-Shang, L. (2017). Effect of TEMPO-oxidization and rapid cooling on thermo-structural properties of nanocellulose. *Carbohydrate Polymers, 173*, 91–99. https://doi.org/10.1016/j.carbpol.2017.05.084
Middleton, S., & Scallan, A. (1985). Lumen-loaded paper pulp: Mechanism of filler-to-fibre bonding. *Journal of Coloids & Surfaces., 16*(3–4), 309–322.
Murizan, N. I. S., Mustafa, N. S., Ngadiman, N. H. A., Mohd Yusof, N., & Idris, A. (2020). Review on nanocrystalline cellulose in bone tissue engineering applications. *Polymers, 12*(12), 2818.
Naderi, Z., Azizian, J., Moniri, E., & Farhadyar, N. (2020). Synthesis and characterization of carboxymethyl cellulose/β-cyclodextrin/chitosan hydrogels and investigating the effect of magnetic nanoparticles (Fe_3O_4) on a novel carrier for a controlled release of methotrexate as drug delivery. *Journal of Inorganic Organometallic Polymers and Materials, 30*(4), 1339–1351.
Nata, I. F., Sureshkumar, M., & Lee, C.-K. (2011). One-pot preparation of amine-rich magnetite/bacterial cellulose nanocomposite and its application for arsenate removal. *RSC Advances, 1*(4), 625–631.
Ng, E. Y. K., & Kumar, S. D. (2017). Physical mechanism and modeling of heat generation and transfer in magnetic fluid hyperthermia through Néelian and Brownian relaxation: A review. *Biomedical Engineering Online, 16*(1), 1–22.
Ni, D., Bu, W., Ehlerding, E. B., Cai, W., & Shi, J. (2017). Engineering of inorganic nanoparticles as magnetic resonance imaging contrast agents. *Chemical Society Reviews, 46*(23), 7438–7468.
Ni, W., Zheng, Z., Liu, H., Wang, P., Wang, L., Wang, H., Sun, X., Yang, Q., Tang, H., & Zhao, G. (2020). Synthesis of the carboxymethyl cellulose magnetic nanoparticles for efficient immobilization of prenyltransferase NovQ. *Carbohydrate Polymers, 235*, 115955.
Nkansah, M. K., Thakral, D., & Shapiro, E. M. (2011). Magnetic poly(lactide-co-glycolide) and cellulose particles for MRI-based cell tracking. *Magnetic Resonance in Medicine, 65*(6), 1776–1785.
Nypelö, T., Rodriguez-Abreu, C., Rivas, J., Dickey, M. D., & Rojas, O. J. (2014). Magneto-responsive hybrid materials based on cellulose nanocrystals. *Cellulose, 21*(4), 2557–2566.
Olsson, N., James, P., Borrebaeck, C. A., & Wingren, C. (2012). Quantitative proteomics targeting classes of motif-containing peptides using immunoaffinity-based mass spectrometry. *Molecular Cellular Proteomics, 11*(8), 342–354.
Pan, Y.-F., Wang, X., Zhang, S.-B., Wang, Y., & Huang, J.-T. (2016). Preparation, formation mechanism and performance of magnetic hollow coatings based on micro/nano cellulose fibers. *Surface and Coatings Technology, 302*, 131–141.
Panchal, P., Ogunsona, E., & Mekonnen, T. (2018). Trends in advanced functional material applications of nanocellulose. *Processes, 7*(1).
Papaparaskeva, G., Dinev, M. M., Krasia-Christoforou, T., Turcu, R., Porav, S. A., Balanean, F., & Socoliuc, V. (2020). White magnetic paper with zero remanence based on electrospun cellulose microfibers doped with iron oxide nanoparticles. *Nanomaterials, 10*(3).
Pardo, A., Pelaz, B., Gallo, J., Bañobre-López, M., Parak, W. J., Barbosa, S., … Taboada, P. (2020). Synthesis, characterization, and evaluation of superparamagnetic doped ferrites as potential therapeutic nanotools. *Chemistry of Materials, 32*(6), 2220–2231.
Pasin, M., Steele, R., & Ferrante, G. (2018). Fast field cycling NMR application: MRI contrast agents. *Magnetic Resonance in Chemistry, 54*(6), 502–509.
Pathak, R., & Kashyap, A. (2021). Boron interstitials in ordered phases of Fe-Pd binary alloys: A first principle study. *Journal of Magnetism Magnetic Materials, 528*, Article 167766.
Peng, F., Yin, H., Cao, S.-L., & Lou, W.-Y. (2019). Enzyme nanocarriers. In *Advances in enzyme technology* (pp. 153–168). Elsevier.
Peng, S., Meng, H. C., Zhou, L., & Chang, J. (2014). Synthesis of novel magnetic cellulose-chitosan composite microspheres and their application in laccase immobilization. *Journal of Nanoscience and Nanotechnology, 14*(9), 7010–7014.
Pham, T. N., Huy, T. Q., & Le, A.-T. (2020). Spinel ferrite (AFe_2O_4)-based heterostructured designs for lithium-ion battery, environmental monitoring, and biomedical applications. *RSC Advances, 10*(52), 31622–31661.
Pislaru, S. V., Harbuzariu, A., Agarwal, G., Witt, T., Gulati, R., Sandhu, N. P., … Sandhu, G. S. (2006). Magnetic forces enable rapid endothelialization of synthetic vascular grafts. *Circulation, 114*(1), I314–I318.
Pourjavadi, A., Tehrani, Z. M., & Moghanaki, A. A. (2016). Folate-conjugated pH-responsive nanocarrier designed for active tumor targeting and controlled release of gemcitabine. *Pharmaceutical Research, 33*(2), 417–432.
Pramanik, S., Agarwala, P., Vasudevan, K., & Sarkar, K. (2019). Human-lymphocyte cell friendly starch–hydroxyapatite biodegradable composites: Hydrophilic mechanism, mechanical, and structural impact. *Journal of Applied Polymer Science, 137*(30), 48913.
Pramanik, S., & Kar, K. K. (2012). Functionalized poly(ether ether ketone): Improved mechanical property and acellular bioactivity. *Journal of Applied Polymer Science, 123*(2), 1100–1111.
Rahimi, M., Shojaei, S., Safa, K. D., Ghasemi, Z., Salehi, R., Yousefi, B., & Shafiei-Irannejad, V. (2017). Biocompatible magnetic tris(2-aminoethyl)amine functionalized nanocrystalline cellulose as a novel nanocarrier for anticancer drug delivery of methotrexate. *New Journal of Chemistry, 41*(5), 2160–2168.
Raymond, L., Revol, J.-F., Ryan, D., & Marchessault, R. (1994). In situ synthesis of ferrites in cellulosics. *Chemistry of Materials, 6*(2), 249–255.
Reddy, L. H., Arias, J. L., Nicolas, J., & Couvreur, P. (2012). Magnetic nanoparticles: Design and characterization, toxicity and biocompatibility, pharmaceutical and biomedical applications. *Chemical Reviews, 112*(11), 5818–5878.
Ryan, A. L., O'Hern, C. P., & Elkins, K. M. (2020). Evaluation of two new methods for DNA extraction of "legal high" plant species. *Journal of Forensic Sciences, 65*(5), 1704–1708.
Sabaqian, S., Nemati, F., Nahzomi, H. T., & Heravi, M. M. (2017). Palladium acetate supported on amidoxime-functionalized magnetic cellulose: Synthesis, DFT study and application in Suzuki reaction. *Carbohydrate Polymers, 177*, 165–177.
Sarkar, T. R., & Irudayaraj, J. (2008). Carboxyl-coated magnetic nanoparticles for mRNA isolation and extraction of supercoiled plasmid DNA. *Analytical Biochemistry, 379*(1), 130–132.
Sattarahmady, N., Heidari, M., Zare, T., Lotfi, M., & Heli, H. (2016). Zinc–nickel ferrite nanoparticles as a contrast agent in magnetic resonance imaging. *Applied Magnetic Resonance, 47*(8), 925–935.
Schlufter, K., Schmauder, H.-P., Dorn, S., & Heinze, T. (2006). Efficient homogeneous chemical modification of bacterial cellulose in the ionic liquid 1-N-Butyl-3-methyl-imidazolium chloride. *Macromolecular Rapid Communications, 27*(19), 1670–1676.
Shahwan, S., Othman, A., Zain, N., Rozali, N. L., & Ramli, U. S. (2020). All-in-one comprehensive extraction of metabolites, proteins and ribonucleic acids for the rapid analysis of oil palm systems biology. *bioRxiv*, 2020.2007.2001.183475.
Sharifi, M., Robatjazi, S.-M., Sadri, M., & Mosaabadi, J. M. (2019). Immobilization of organophosphorus hydrolase enzyme by covalent attachment on modified cellulose microfibers using different chemical activation strategies: Characterization and stability studies. *Chinese Journal of Chemical Engineering, 27*(1), 191–199.
Shende, P., & Shah, P. (2021). Carbohydrate-based magnetic nanocomposites for effective cancer treatment. *International Journal of Biological Macromolecules., 175*(1), 281–293.
Sitthichai, S., Pilapong, C., Thongtem, T., & Thongtem, S. (2015). CMC-coated Fe_3O_4 nanoparticles as new MRI probes for hepatocellular carcinoma. *Applied Surface Science, 356*, 972–977.
Sivakumar, B., Aswathy, R. G., Nagaoka, Y., Suzuki, M., Fukuda, T., Yoshida, Y., … Sakthikumar, D. N. (2013). Multifunctional carboxymethyl cellulose-based magnetic nanovector as a theragnostic system for folate receptor targeted chemotherapy, imaging, and hyperthermia against cancer. *Langmuir, 29*(10), 3453–3466.
Su, R., Wang, F., Ding, J., Li, Q., Zhou, W., Liu, Y., Gao, B., & Yue, Q. (2019). Magnetic hydrogel derived from wheat straw cellulose/feather protein in ionic liquids as copper nanoparticles carrier for catalytic reduction. *Carbohydrate Polymers, 220*, 202–210.
Sun, X., Wang, Y., Zhang, L., Liu, S., Zhang, M., Wang, J., … Hu, Y. (2020). CRISPR-Cas9 triggered two-step isothermal amplification method for E. coli O157: H7 detection based on a metal–organic framework platform. *Analytical Chemistry, 92*(4), 3032–3041.
Sunderland, C. J., Steiert, M., Talmadge, J. E., Derfus, A. M., & Barry, S. E. (2006). Targeted nanoparticles for detecting and treating cancer. *Drug Development Research, 67*(1), 70–93.
Supramaniam, J., Adnan, R., Mohd Kaus, N. H., & Bushra, R. (2018). Magnetic nanocellulose alginate hydrogel beads as potential drug delivery system. *International Journal of Biological Macromolecules, 118*(Part A), 640–648.
Taghizadeh, M. T., Ashassi-Sorkhabi, H., Afkari, R., & Kazempour, A. (2019). Cross-linked chitosan in nano and bead scales as drug carriers for betamethasone and tetracycline. *International Journal of Biological Macromolecules, 131*, 581–588.
Tamaddon, F., Arab, D., & Ahmadi-AhmadAbadi, E. (2020). Urease immobilization on magnetic micro/nano-cellulose dialdehydes: Urease inhibitory of Biginelli product in Hantzsch reaction by urea. *Carbohydrate Polymers, 229*, 15471.

Tan, S. C., & Yiap, B. C. (2009). DNA, RNA, and protein extraction: The past and the present. *BioMed Research International, 2009*, 574398.
Tao, H., Lavoine, N., Jiang, F., Tang, J., & Lin, N. (2020). Reducing end modification on cellulose nanocrystals: Strategy, characterization, applications and challenges. *Nanoscale Horizons, 5*(4), 607–627.
Thapar, U., & Demple, B. (2019). Deployment of DNA polymerases beta and lambda in single-nucleotide and multinucleotide pathways of mammalian base excision DNA repair. *DNA Repair, 76*, 11–19.
Torgbo, S., & Sukyai, P. (2019). Fabrication of microporous bacterial cellulose embedded with magnetite and hydroxyapatite nanocomposite scaffold for bone tissue engineering. *Materials Chemistry and Physics, 237*, Article 121868.
Torkashvand, N., & Sarlak, N. (2019). Fabrication of a dual T1 and T2 contrast agent for magnetic resonance imaging using cellulose nanocrystals/Fe_3O_4 nanocomposite. *European Polymer Journal, 118*, 128–136.
Turyanska, L., Makarovsky, O., Patane, A., Kozlova, N. V., Liu, Z., Li, M., & Mann, S. (2012). High magnetic field quantum transport in Au nanoparticle-cellulose films. *Nanotechnology, 23*(4), Article 045702.
Ulbrich, K., Hola, K., Subr, V., Bakandritsos, A., Tucek, J., & Zboril, R. (2016). Targeted drug delivery with polymers and magnetic nanoparticles: Covalent and noncovalent approaches, release control, and clinical studies. *Chemical Reviews, 116*(9), 5338–5431.
Umar, A. A., Saaid, I. M., Halilu, A., Sulaimon, A. A., & Ahmed, A. A. (2020). Magnetic polyester bis-MPA dendron nanohybrid demulsifier can effectively break water-in-crude oil emulsions. *Journal of Materials Research Technology, 9*(6), 13411–13424.
Vamvakidis, K., Sakellari, D., Angelakeris, M., & Dendrinou-Samara, C. (2013). Size and compositionally controlled manganese ferrite nanoparticles with enhanced magnetization. *Journal of Nanoparticle Research, 15*(6), 1–11.
Verma, S. K., & Biswas, N. (2020). A novel nucleic acid extraction method from aromatic herbs and dried herbal powders using cow skim milk. *Scientific Reports, 10*(1), 1–8.
Wågberg, L. (2000). Polyelectrolyte adsorption onto cellulose fibres–A review. *Nordic PulpPaper Research Journal, 15*(5), 586–597.
Wan, C., & Li, J. (2015). Synthesis of well-dispersed magnetic $CoFe_2O_4$ nanoparticles in cellulose aerogels via a facile oxidative co-precipitation method. *Carbohydrate Polymers, 134*, 144–150.
Wang, F., Yang, Y., Ling, Y., Liu, J., Cai, X., Zhou, X., Tang, X., Liang, B., Chen, Y., Chen, H., Chen, D., Li, C., Wang, Z., Hu, B., & Zheng, Y. (2017). Injectable and thermally contractible hydroxypropyl methyl cellulose/Fe_3O_4 for magnetic hyperthermia ablation of tumors. *Biomaterials, 128*, 84–93.
Wang, Q., Jamal, S., Detamore, M. S., & Berkland, C. (2011). PLGA-chitosan/PLGA-alginate nanoparticle blends as biodegradable colloidal gels for seeding human umbilical cord mesenchymal stem cells. *Journal of Biomedical Materials Research Part A, 96*(3), 520–527.
Wang, X., Zhao, L., Wu, X., Luo, H., Wu, D., Zhang, M., Zhang, J., Pakvasa, M., Wagstaff, W., & He, F. (2020). Development of a simplified and inexpensive RNA depletion method for plasmid DNA purification using size selection magnetic beads (SSMBs). *Genes Diseases, 8*(3), 298–306.
Wang, X., Han, B., Yu, R.-P., Li, F.-C., Zhao, Z.-Y., Zhang, Q.-C., & Lu, T. J. (2018). Magnetic-responsive Fe3O4 nanoparticle-impregnated cellulose paper actuators. *Extreme Mechanics Letters, 25*, 53–59.
Wang, X., Zhao, L., Wu, X., Luo, H., Wu, D., Zhang, M., … He, F. (2020). Development of a simplified and inexpensive RNA depletion method for plasmid DNA purification using size selection magnetic beads (SSMBs). *Genes Diseases* (In Press).
Wijaya, C. J., Ismadji, S., & Gunawan, S. (2021). A review of lignocellulosic-derived nanoparticles for drug delivery applications: Lignin nanoparticles, xylan nanoparticles, and cellulose nanocrystals. *Molecules, 26*(3), 676.
Williams, S., Okolie, C. L., Deshmukh, J., Hawco, L., McNeil, J., Nganou Assonkeng, A. C., … Mkandawire, M. (2019). Magnetizing cellulose fibers with $CoFe_2O_4$ nanoparticles for smart wound dressing for healing monitoring capability. *ACS Applied Bio Materials., 2*(12), 5653–5662.
Xin, Y., Wang, G., Han, W., Shen, Y., & Uyama, H. (2018). An ideal enzyme immobilization carrier: A hierarchically porous cellulose monolith fabricated by phase separation method. *Pure and Applied Chemistry, 90*(6), 1055–1062.
Xiong, J., Cao, S.-L., Zong, M.-H., Lou, W.-Y., & Wu, X.-l. (2020). Biosynthesis of alanyl-histidine dipeptide catalyzed by papain immobilized on magnetic nanocrystalline cellulose in deep eutectic solvents. *Applied Biochemistry and Biotechnology, 192*, 573–584.
Xiong, R., Lu, C., Wang, Y., Zhou, Z., & Zhang, X. (2013). Nanofibrillated cellulose as the support and reductant for the facile synthesis of Fe_3O_4/Ag nanocomposites with catalytic and antibacterial activity. *Journal of Materials Chemistry A, 1*(47), 14910.
Xue, F., Chen, Q., Li, Y., Liu, E., & Li, D. (2019). Immobilized lysozyme onto 1,2,3,4-butanetetracarboxylic (BTCA)-modified magnetic cellulose microsphere for improving bio-catalytic stability and activities. *Enzyme and Microbial Technology, 131*, 109425.
Yamazaki, M., Hosokawa, M., Arikawa, K., Takahashi, K., Sakanashi, C., Yoda, T., Matsunaga, H., & Takeyama, H. (2020). Effective microtissue RNA extraction coupled with Smart-seq2 for reproducible and robust spatial transcriptome analysis. *Scientific Reports, 10*(1), 1–8.
Yang, J., & Li, J. (2018). Self-assembled cellulose materials for biomedicine: A review. *Carbohydrate Polymers, 181*, 264–274.
Yang, W., Tian, H., Liao, J., Wang, Y., Liu, L., Zhang, L., & Lu, A. (2020). Flexible and strong Fe_3O_4/cellulose composite film as magnetic and UV sensor. *Applied Surface Science, 507*, 145092.
Yee, Y. C., Hashim, R., Mohd Yahya, A. R., & Bustami, Y. (2019). Colorimetric analysis of glucose oxidase-magnetic cellulose nanocrystals (CNCs) for glucose detection. *Sensors (Basel), 19*(11), 2511.
Yoshitake, H., Sugimura, K., Teramoto, Y., & Nishio, Y. (2016). Magnetic property of oriented films of cellulose nanocrystal/carrageenan composites containing iron oxide nanoparticles: Effect of anisotropic aggregation of the nanoparticles. *Polymer, 99*, 147–156.
Zavala-Alvarado, C., & Benaroudj, N. (2020). The single-step method of rna purification applied to leptospira. Leptospira spp. In , *Vol 2134. Methods in molecular biology* (pp. 41–51). Humana, New York, NY: Springer.
Zengin Kurt, B., Uckaya, F., & Durmus, Z. (2017). Chitosan and carboxymethyl cellulose based magnetic nanocomposites for application of peroxidase purification. *International Journal of Biological Macromolecules, 96*, 149–160.
Zhan, Y., Meng, Y., Li, W., Chen, Z., Yan, N., Li, Y., & Teng, M. (2018). Magnetic recoverable MnFe2O4/cellulose nanocrystal composites as an efficient catalyst for decomposition of methylene blue. *Industrial Crops and Products, 122*, 422–429.
Zhang, B., Huang, C., Zhao, H., Wang, J., Yin, C., Zhang, L., & Zhao, Y. J. P. (2019). Effects of cellulose nanocrystals and cellulose nanofibers on the structure and properties of polyhydroxybutyrate nanocomposites. *Polymers, 11*(12), 2063.
Zhang, F., Wang, R., Zhen, C., & Li, B. (2016). Magnetic cellulose nanocrystals: Synthesis by electrostatic self-assembly approach and efficient use for immobilization of papain. *Journal of Molecular Catalysis B: Enzymatic, 134*, 164–171.
Zhang, H., Hua, S. F., & Zhang, L. (2020). Co-immobilization of cellulase and glucose oxidase on graphene oxide by covalent bonds: A biocatalytic system for one-pot conversion of gluconic acid from carboxymethyl cellulose. *Journal of Chemical Technology & Biotechnology, 95*(4), 1116–1125.
Zhang, H., Liu, T., Zhu, Y., Hong, L., Li, T., Wang, X., & Fu, Y. (2020). Lipases immobilized on the modified polyporous magnetic cellulose support as an efficient and recyclable catalyst for biodiesel production from Yellow horn seed oil. *Renewable Energy, 145*, 1246–1254.
Zhang, L., Liu, Y., Zhang, Q., Li, T., Yang, M., Yao, Q., … Hu, H. Y. (2018). Gadolinium-labeled aminoglycoside and its potential application as a bacteria-targeting magnetic resonance imaging contrast agent. *Analytical Chemistry, 90*(3), 1934–1940.
Zhang, W., Jin, X., Li, H., Zhang, R.-R., & Wu, C.-W. (2018). Injectable and body temperature sensitive hydrogels based on chitosan and hyaluronic acid for pH sensitive drug release. *Carbohydrate Polymers, 186*, 82–90.
Zhao, F., Lee, E. Y., & Shin, Y. (2018). Improved reversible cross-linking-based solid-phase rna extraction for pathogen diagnostics. *Analytical Chemistry, 90*(3), 1725–1733.
Zhao, Z., Cui, H., Song, W., Ru, X., Zhou, W., & Yu, X. (2020). A simple magnetic nanoparticles-based viral RNA extraction method for efficient detection of SARS-CoV-2. *bioRxiv*, 2020.2002.2022.961268.
Zhou, Z., Huang, D., Bao, J., Chen, Q., Liu, G., Chen, Z., … Gao, J. (2012). A synergistically enhanced T(1)-T(2) dual-modal contrast agent. *Advanced Materials, 24*(46), 6223–6228.
Zhu, C., Varona, M., & Anderson, J. L. (2020). Magnetic ionic liquids as solvents for RNA extraction and preservation. *ACS Omega, 5*(9), 11151–11159.

View publication stats